TWO-DIMENSIONAL SUBSONIC EXPERIMENTS WITH AN NACA 0012 AIRFOIL

R. J. Vidal, et al

Calspan Corporation

Prepared for:

Office of Naval Research
Air Force Office of Scientific Research

December 1973

Calspan

Technical Report

TWO-DIMENSIONAL SUBSONIC EXPERIMENTS WITH AN NACA 0012 AIRFOIL

R.J. Vidal, P.A. Catlin, and D.W. Chudyk

Calspan Report No. RK-5070-A-3

Calspan Corporation
Buffalo, New York 14221

AD775 880

Calspan

On November 17, 1972 Cornell Aeronautical Laboratory (CAL) changed its name to Calspan Corporation and converted to for-profit operations. Calspan is dedicated to carrying on CAL's long-standing tradition of advanced research and development from an independent viewpoint. All of CAL's diverse scientific and engineering programs for government and industry are being continued in the aerosciences, electronics and avionics, computer sciences, transportation and vehicle research, and the environmental sciences. Calspan is composed of the same staff, management, and facilities as CAL, which operated since 1946 under federal income tax exemption.

TWO-DIMENSIONAL SUBSONIC EXPERIMENTS WITH AN NACA 0012 AIRFOIL

R.J. Vidal, P.A. Catlin, and D.W. Chudyk

Calspan Report No. RK-5070-A-3

Prepared For:

UNITED STATES NAVY
OFFICE OF NAVAL RESEARCH
AND
UNITED STATES AIR FORCE
OFFICE OF SCIENTIFIC RESEARCH

DECEMBER 1973
CONTRACT NO. N00014-72-C-0102
PROJECT NO. NR 061-199/09-08-71 (438)
TECHNICAL REPORT

PREPARED BY: R.J. Vidal
R.J. Vidal

P.A. Catlin
P.A. Catlin

D.W. Chudyk
D.W. Chudyk

APPROVED BY: Alfred Ritter
Alfred Ritter, Assistant Head
Aerodynamic Research Department

53

Calspan Corporation
Buffalo, New York 14221

PREFACE

This report is based on research carried out at Calspan Corporation under Contract No. N00014-72-C-0102, Project No. NR 061-199/09-08-71(438). This research is sponsored jointly by the Office of Naval Research, with Mr. Morton Cooper as technical monitor, and the Air Force Office of Scientific Research, with Mr. Milton Rogers as technical monitor. The authors wish to acknowledge the contributions of Prof. W. R. Sears of Cornell University who originated the concept of a self-correcting wind tunnel. Prof. Sears is a consultant to Calspan on this contract. Calspan personnel who have contributed to this research include Dr. John C. Erickson, Jr., Mr. Joseph P. Nenni, and Dr. William J. Rae.

UNCLASSIFIED

SECURITY CLASSIFICATION OF THIS PAGE *(When Data Entered)*

REPORT DOCUMENTATION PAGE		READ INSTRUCTIONS BEFORE COMPLETING FORM
1. REPORT NUMBER RK-5070-A-3	2. GOVT ACCESSION NO.	3. RECIPIENT'S CATALOG NUMBER
4. TITLE *(and Subtitle)* TWO-DIMENSIONAL SUBSONIC EXPERIMENTS WITH AN NACA 0012 AIRFOIL		5. TYPE OF REPORT & PERIOD COVERED Technical Report 6. PERFORMING ORG. REPORT NUMBER RK-5070-A-3
7. AUTHOR(s) R. J. Vidal, P. A. Catlin, D. W. Chudyk		8. CONTRACT OR GRANT NUMBER(s) N00014-72-C-0102
9. PERFORMING ORGANIZATION NAME AND ADDRESS Calspan Corporation P. O. Box 235 Buffalo, New York 14221		10. PROGRAM ELEMENT, PROJECT, TASK AREA & WORK UNIT NUMBERS NR 061-199/09-08-71(438)
11. CONTROLLING OFFICE NAME AND ADDRESS USN Office of Naval Research and USAF Office of Scientific Research		12. REPORT DATE December 1973 13. NUMBER OF PAGES 60
14. MONITORING AGENCY NAME & ADDRESS*(if different from Controlling Office)*		15. SECURITY CLASS. *(of this report)* Unclassified 15a. DECLASSIFICATION/DOWNGRADING SCHEDULE

16. DISTRIBUTION STATEMENT *(of this Report)*

Reproduction in whole or in part is permitted for any purpose of the United States Government. Approved for public release; distribution unlimited.

17. DISTRIBUTION STATEMENT *(of the abstract entered in Block 20, if different from Report)*

18. SUPPLEMENTARY NOTES

19. KEY WORDS *(Continue on reverse side if necessary and identify by block number)*

NACA 0012, Two-dimensional experiments, Subsonic, Transonic, Wind tunnel

20. ABSTRACT *(Continue on reverse side if necessary and identify by block number)*

Two-dimensional tests were made with a 6-inch chord NACA 0012 section in the Calspan 8-foot Transonic Wind Tunnel to obtain section data with minimum wall interference effects. The measurements included three - component force data, surface pressure distributions and oil flow observations, and were made at Mach numbers ranging from 0.4 to 0.95 and at a chord Reynolds number of 10^6. Comparisons of the lift curve data with available theory indicate that the results are within about 1% of being two-dimensional. The slopes of the lift curves near

DD FORM 1 JAN 73 1473 EDITION OF 1 NOV 65 IS OBSOLETE

UNCLASSIFIED

SECURITY CLASSIFICATION OF THIS PAGE *(When Data Entered)*

zero angle of attack are very small at Mach numbers between 0.85 and 0.925 because of shock wave formation on the surface. The profile drag increased about 14% in the subcritical Mach number range. It is shown that this increase is due to inviscid compressibility effects on the viscous and/or pressure drag, and that Prandtl-Glauert scaling applied to a component of the profile drag.

TABLE OF CONTENTS

LIST OF SYMBOLS

AR	Aspect ratio
c	Chord
C_d	Section drag coefficient
C_l	Section lift coefficient
C_m	Section moment coefficient about $\frac{c}{4}$ positive nose up
C_p	Pressure coefficient, $\frac{p - p_\infty}{\frac{1}{2} \rho_\infty U_\infty^2}$
d	Section drag
l	Section lift
M	Mach number
p	Pressure
Re	Reynolds number, $\frac{\rho_\infty U_\infty c}{\mu_\infty}$
s	Surface length
t	Airfoil thickness
U	Velocity
Δu	Disturbance velocity
x	Streamwise coordinate
y	Coordinate normal to the stream
α	Geometric angle of attack
α_e	Effective angle of attack

β	$\sqrt{1 - M_\infty^2}$
δ	Boundary layer thickness
θ	Local surface inclination
μ	Viscosity
ρ	Density
τ	Viscous shear stress

Subscripts

e	Conditions at edge of the boundary layer
i	Incompressible
w	Conditions at the wall
∞	Conditions at infinity

LIST OF FIGURES

INTRODUCTION

A program of research is in progress at the Calspan Corporation to demonstrate theoretically and experimentally the feasibility of controlling the flow through the walls of a ventilated transonic wind tunnel in order to minimize the wall interference effects on a model in the test section. The basic concept of this self-adjusting wind tunnel has been described by Sears.[1] Briefly stated, it is based upon measuring the components of the disturbance velocity field and determining if each is consistent with the boundary condition that all disturbances vanish at infinity.

The present initial effort is restricted to two-dimensional flow and centers on experiments with an NACA 0012 airfoil section in the Calspan One-Foot Wind Tunnel. An important consideration in this demonstration experiment is to verify that unbounded flow conditions have been achieved and that interference-free data have been recorded. This will be accomplished by comparing airfoil data obtained in the One-Foot Wind Tunnel with experimental data known to be free of wall interference effects. This body of interference-free data was obtained in tests in the Calspan Eight-Foot Transonic Wind Tunnel with the same airfoil model being used in the One-Foot Wind Tunnel.

The purpose of this report is to describe the experiments made in the Eight-Foot Wind Tunnel. In the following sections a description is given of the model, the design of the experiment, and the tests in the Eight-Foot Wind Tunnel, and this is followed by a discussion of the experimental results. These results show that the experimental data are within about 1% of being two-dimensional, the sub-critical data are in good agreement with scaled incompressible theory, the data are in good agreement with other experimental results, this airfoil has unusual characteristics at small angles of attack for Mach numbers between 0.8 and 0.925, and that Prandtl-Glauert scaling applies to a component of the profile drag.

THE EIGHT-FOOT TUNNEL EXPERIMENTS

The Calspan Fight-Foot Transonic Wind Tunnel

This wind tunnel is a closed circuit, continuous flow facility that can be operated at total pressures ranging nominally from 1/6-of an atmosphere to 3-1/2-atmospheres, and over a speed range from about five feet per second to a maximum Mach number of about 1.35. It has a test section 8-ft. by 8-ft. square with porous walls that have a 22-1/2% open area. The porosity is formed by 1/2-inch holes drilled normal to the surface of 1/2-inch thick plates. The plenum surrounding the test section is pumped separately by an auxiliary compressor system, and the normal mode of operation is to use this auxiliary pumping, in conjunction with moveable side walls, to maintain a uniform axial pressure distribution in the test section.

There are several test section configurations available for the Eight-Foot Tunnel. That used in the present experiments was the reflection plane cart, illustrated in Figure 1. The test section floor includes a solid section that is 2-1/2 inches above the porous section ahead of it to produce a boundary layer bleed. The boundary layer thickness at the model location is about one-inch. There is a turntable in the center of the solid floor that is used to change the model angle of attack. This turntable angle was calibrated prior to the present experiments, and the geometric angle with respect to the tunnel center line was established with an accuracy of about 0.01°. A complete description of the Eight-Foot Wind Tunnel is given in Ref. 2, and detailed airflow calibrations for the tunnel with the reflection plane cart are given in Ref. 3.

The Model and Experimental Design

The model used was a two-dimensional airfoil with an NACA 0012 section. This section was chosen because there is considerable current interest in the transonic characteristics of this section. It is widely used

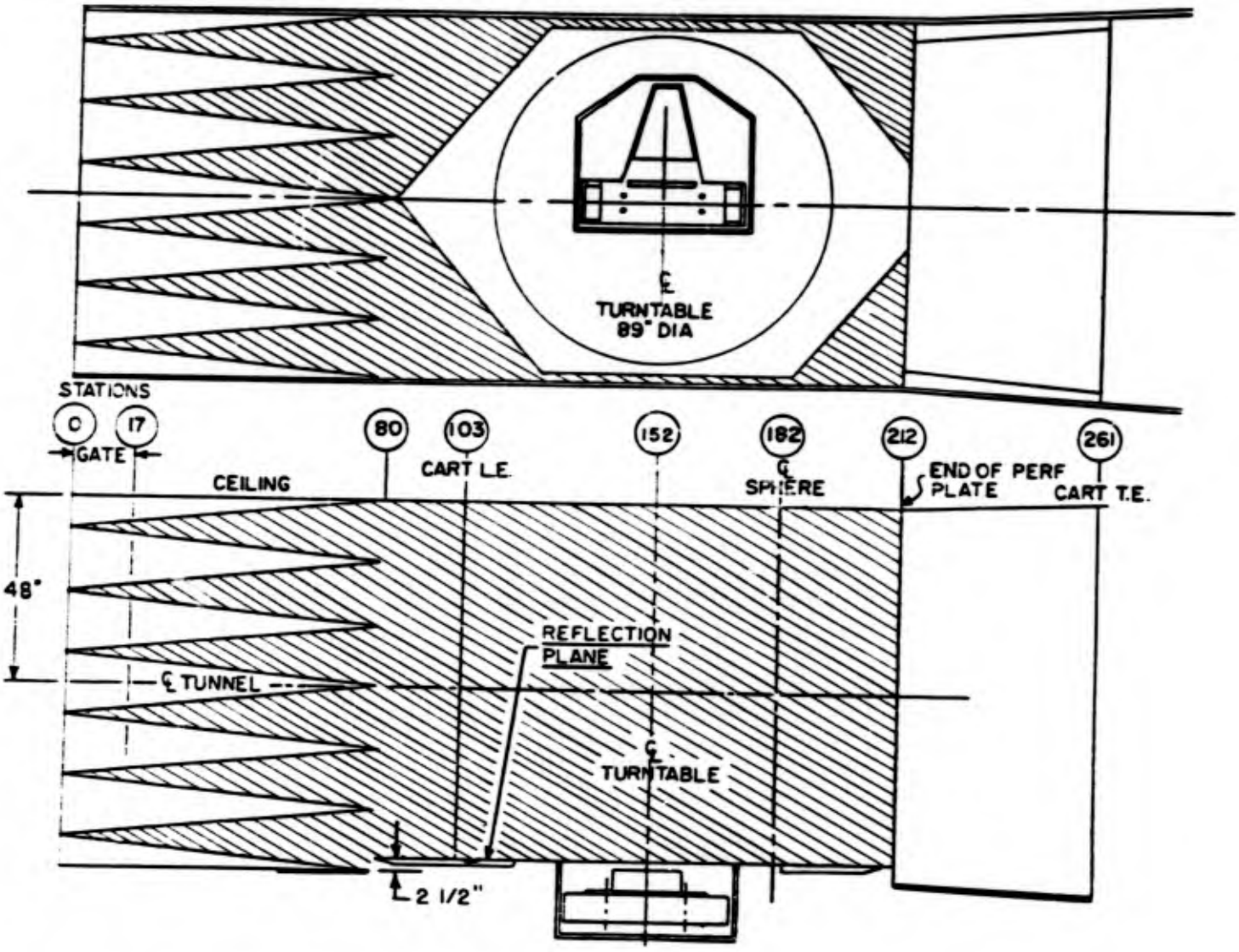

Figure 1 SCHEMATIC DRAWING OF REFLECTION PLANE CART INSTALLATION

for helicopter rotors; it has been selected by AGARD as standard to be used in testing numerical solutions;[4] a significant body of experimental work is in progress[5,6] to determine the airfoil characteristics at transonic speeds; and exact solutions are available for this section.[4,7,25]

It was decided to perform the two-dimensional experiments in the Eight-Foot Wind Tunnel using a finite span airfoil mounted on the reflection plane cart and using an end-plate that spanned the wind tunnel. In effect, the solid floor of the wind tunnel and the end-plate formed a two-dimensional porous-wall channel. The airfoil model has a six-inch chord and a span of 48-inches. This chord length was selected so that it was half the height of the One-Foot Wind Tunnel, and consequently there should be large wall interference effects in that wind tunnel. The span was selected on the basis of the experimental results given in Ref. 8. Those tests were made with a wing of aspect ratio three with end plates spanning the tunnel and extending 1/3 chord length forward of the leading edge and 2/3 chord length aft of the trailing edge. It was concluded there that those end plates effectively increased the aspect ratio by a factor of nine. Application of those results directly to our experiment indicated that the effective aspect ratio would be about 72. Since our measurements were to be made near the tunnel floor, it was effectively a semi-span model with an effective ratio approaching 144. Using the theory of Ref. 9, it can be shown that the effective angle of attack of a rectangular wing at its midspan is $\frac{\alpha_e}{\alpha} = 1 - \frac{1}{AR}$ where AR is the aspect ratio. Consequently, the present data were expected to be within about 1% of the two-dimensional values. It should be noted that this is probably a conservative estimate since the end plate used here extended 2 chord lengths forward and aft of the airfoil leading and trailing edges and hence is considerably larger in chord length than those used in Ref. 8.

The forces on the model were measured on a metric section 2-1/2 inches wide with a three-component balance contained within that section and supported in the nonmetric portion. A gap of 1/16-inch was left on each side of the metric section, and was sealed by wrapping the model at the metric

section with 0.005-inch thick dental dam rubber. This type of model construction had been used previously[10] with good success. The metric section was located about two chord lengths from the solid floor of the reflection plane cart. A total of 46 pressure orifices were located on the nonmetric section about one-inch from the gap to obtain the airfoil pressure distribution. The balance was calibrated with and without the rubber seal. It was found that without the rubber seal, the repeatability for all three components was better than 0.1%. With the seal in place, the repeatability was 0.5%, 0.25%, and 0.6% for the normal force, the axial force, and the pitching moment, respectively.

The wall interference effects on the model in the Eight-Foot-Transonic Wind Tunnel were estimated using the theory of Ref. 11 and assuming the wall loss characteristics were those given in Ref. 12. These estimates showed that the blockage interference should alter the free-stream velocity by less than 0.1%. The lift interference on the model was less than 2% for all Mach numbers considered, and it was an open-jet type of interference.

Transition strips were mounted on the upper and lower surface of the model. These were selected using the criteria of Ref. 13 and were made with No. 100 grit (0.0059-inch diameter particles) located between $x/c = 0.10$ and $x/c = 0.108$.

The model mounted in the test section is shown in Figs. 2 and 3. It was mounted on the floor turntable and pinned at the splitter plate to minimize torsional deflections and the attendant uncertainties in angle of attack. There is a boundary layer bleed upstream of the mounting point, and the boundary layer thickness at the model position is about one-inch. It can be seen in Figs. 2 and 3 that porous plates were fitted on the floor around the model root, and the cavity behind the plates was vented to the suction plenum. These were included in the apparatus in an attempt to stabilize the boundary layer at this junction and to prevent an adverse separation. The first experiment showed that the plenum suction was inadequate, and that there was flow from the plenum into the test section through these

Figure 2 VIEW OF 0012 TWO-DIMENSIONAL MODEL FROM DOWNSTREAM

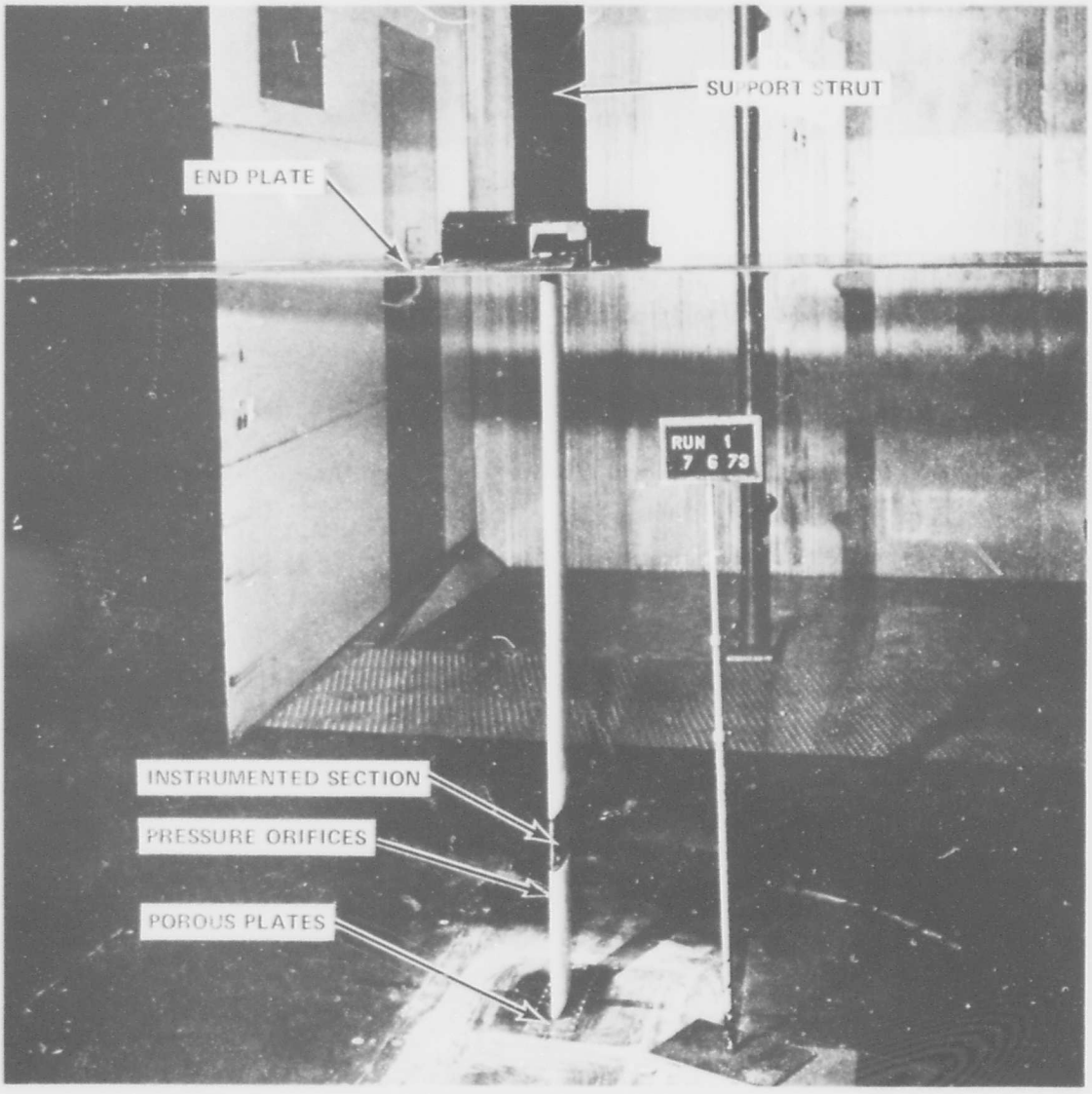

Figure 3 VIEW OF 0012 TWO-DIMENSIONAL MODEL FROM UPSTREAM

porous inserts. All subsequent experiments were performed with the perforations sealed off. The flow-field near the model-wall junction was monitored with oil film photographs throughout the experiments, and no unusual separation effects were observed.

Experimental Mode of Operation

The experiments were run in two phases. In the first phase, the test section flow was calibrated with the end plate and support strut installed, Fig. 3, and with a static pressure pipe mounted in the test at a vertical position corresponding to the location of the airfoil metric section. It was found that the Mach number variations in the axial region defined by the end plate typically was 0.005 for all Mach numbers up to 0.95. This corresponds to a static pressure variation of 1/2% to 1%, depending on the Mach number. At Mach numbers of 1.0 and above, the vertical support strut above the end plate apparently choked the flow and produced a detached shock wave that resulted in an expansion at the leading edge of the end plate. The resulting flow at the model location was unacceptable, and the experiments were limited to a maximum Mach number of 0.95. All Mach numbers are those at the model position and are based upon the static pressure calibration.

The Mach numbers and angles of attack covered in the experiments are listed in the table. The method of operation was to set the model angle of attack manually and to run through the Mach number range, taking oil.flow photographs, without attempting to control the Reynolds number. Force and pressure data were then taken at a constant Reynolds number of 2×10^6 per foot, starting at the highest Mach number.

Table I Test Conditions

Mach Numbers	Angles of Attack
0.40	-2
0.55	-1
0.65	0
0.725	1
0.75	2
0.80	3
0.85	4
0.90	6
0.925	8
0.95	

EXPERIMENTAL RESULTS

Lift

The slopes of the lift curves near zero angle of attack are plotted in Fig. 4 against Mach number to test the two-dimensionality of the experiment. These data show the expected compressibility effect causing the lift curve slope to increase up to a Mach number of 0.80. A strong shock wave is present on the airfoil above that Mach number, causing a pronounced loss in lift at small angles of attack. A similar behavior was observed by Goethert[14,15] in tests on an NACA 0012-1.1 airfoil. The additional numerical designation is the DVL confirmation of the NACA profile, but the ordinates tabulated by Goethert differ slightly from those given in Ref. 16, the ones used here. He reports in Ref. 14 that his airfoil had an aspect ratio of 2.6 with elliptical end plates 1.2 chords high and 2.2 chords in length. He reports an incompressible lift curve slope in Ref. 14 that is about 97% of the theoretical value shown in Fig. 4. However, in Ref. 15 he reports data, presumably from the same airfoil, that is 83% of this theoretical value. Regardless of this point, he also finds that the lift curve slope increases slightly less than the Prandtl-Glauert prediction up to $M_\infty = 0.80$ and it then falls to slightly less than the imcompressible value at $M_\infty = 0.85$. The differences between his results and the present results probably stem from the fact his chord Reynolds number varied from 2.3×10^6 at $M = 0.2$ to 6.3×10^6 at $M = 0.80$. In contrast, the present results were obtained at a constant Reynolds number, 10^6, and with a boundary layer trip.

The lift curve slopes in Fig. 4 have been scaled to an imcompressible value using the Prandtl-Glauert scaling, $(C_{\ell_\alpha})_i = \beta C_{\ell_\alpha}$. In addition, the von Kármán-Tsien scaling was applied in the following approximate fashion. This scaling for the pressure coefficient was cast into the following form:

$$\beta C_p = C_{p_i} - \frac{M_\infty^2}{1+\beta} \frac{C_{p_i} C_p}{2} \qquad (1)$$

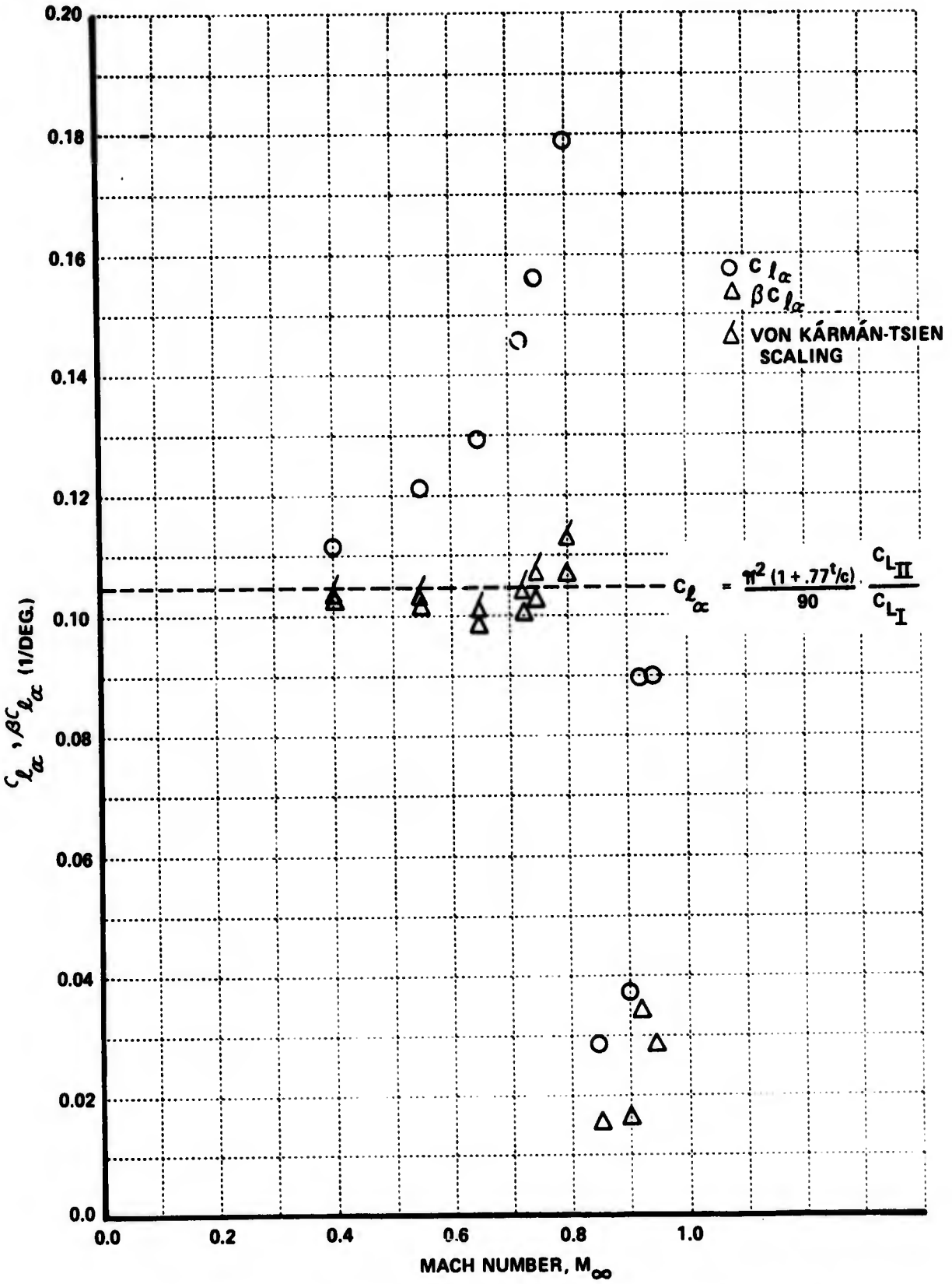

Figure 4 LIFT CURVE SLOPES AT ZERO ANGLE OF ATTACK

where the subscript, i, refers to the incompressible value. Noting that the second term on the right is a small second-order term, Prandtl-Glauert scaling was applied to replace the compressible pressure coefficient, and the integration was performed around the airfoil to obtain the following correction

$$(C_\ell)_i = \frac{\beta C_\ell}{1 - \frac{M_\infty^2}{2\beta(1+\beta)} \oint \frac{(C_{p_i})^2}{C_{\ell_i}} d\left(\frac{x}{c}\right)} \qquad (2)$$

This form of the von Kármán-Tsien scaling was applied to the data at $\pm$ 1° angle of attack to obtain the scaled lift curve slopes in Fig. 4.

The theoretical estimate of the incompressible lift curve slope shown in Fig. 4 is based upon the theoretical characteristics of a Joukowski airfoil approximately 12% thick. It includes the classical thickness correction, $(1 + 0.77\frac{t}{c})$, taken, for example, from Glauert.[17] It also includes a second-order viscous correction, $C_{\ell_{II}} / C_{\ell_I}$, obtained by Spence[18] and as reported by Thwaites.[19] This correction accounts for the displacement effect of the boundary layer and the wake on the inviscid flow field, and was derived for an 11.8% thick Joukowski airfoil. The correction, as given by Thwaites, is $C_{\ell_{II}} / C_{\ell_I} = 0.876$ and it multiplies the total inviscid lift, including the thickness effect. It is interesting to note that Spence regards this correction as second-order in comparison with the first-order thickness correction. However, the viscous correction is slightly than the thickness correction.

The scaled slopes of the lift curves shown in Fig. 4 are seen to be in good agreement with the theoretical incompressible value for Mach numbers of 0.8 or less. As expected, the best agreement is at the lowest Mach number, 0.40, and the data scaled with the Prandtl-Glauert correction fall about 1.7% below theory. The von Kármán-Tsien scaling improves the agreement to within about 1.0%. This comparison indicates that the present experiments were closely two-dimensional.

The lift curves for all of the Mach numbers are presented in Figs. 5(a) and 5(b), and the lift coefficient at which the airfoil becomes supercritical is indicated by a symbol. These supercritical points are theoretical values obtained from Ref. 16, and are based on scaling the incompressible theory with the von Kármán-Tsien correction. First, it should be noted that apparently there was a slight flow angularity in the wind tunnel which increased from nominally zero at $M_\infty = 0.4$ to about 0.2° at $M_\infty = 0.95$, with the exception of a reversal at $M_\infty = 0.90$. This angularity, however, does not interfere with the objective of the present program.

The lift curves at the lower Mach numbers, $M_\infty = 0.4$ to 0.725, show the expected compressibility effects and indicate no unusual effects when the theoretical supercritical lift coefficient is exceeded. The stall occurs at lower lift coefficients as the Mach number is increased, and the $M_\infty = 0.8$ data indicate that the lift curve is strongly affected by shock waves on the surface which degrade the lift but do not produce stall. The data at $M_\infty = 0.85$ and 0.90 illustrate the behavior noted in Fig. 4 in that the lift curve slope is very small near zero lift. Figure 5 shows that the lift curves approach a more normal behavior at higher angles of attack and at higher Mach numbers.

Drag

The drag data obtained at zero angle of attack are presented in Fig. 6 and show a marked increase in drag for Mach numbers greater than 0.75, indicating the presence of strong shock waves on the airfoil. This drag rise begins at Mach numbers slightly higher than the theoretical critical Mach number of 0.725.

The data in Fig. 6 also show that there is an increase of about 14% in the drag in the subcritical Mach number range between $M_\infty = 0.4$ and 0.725. It is believed that this subcritical drag rise stems from inviscid compressibility effects that increase the viscous and/or pressure drag on the airfoil. This can be demonstrated in an approximate fashion by writing down the

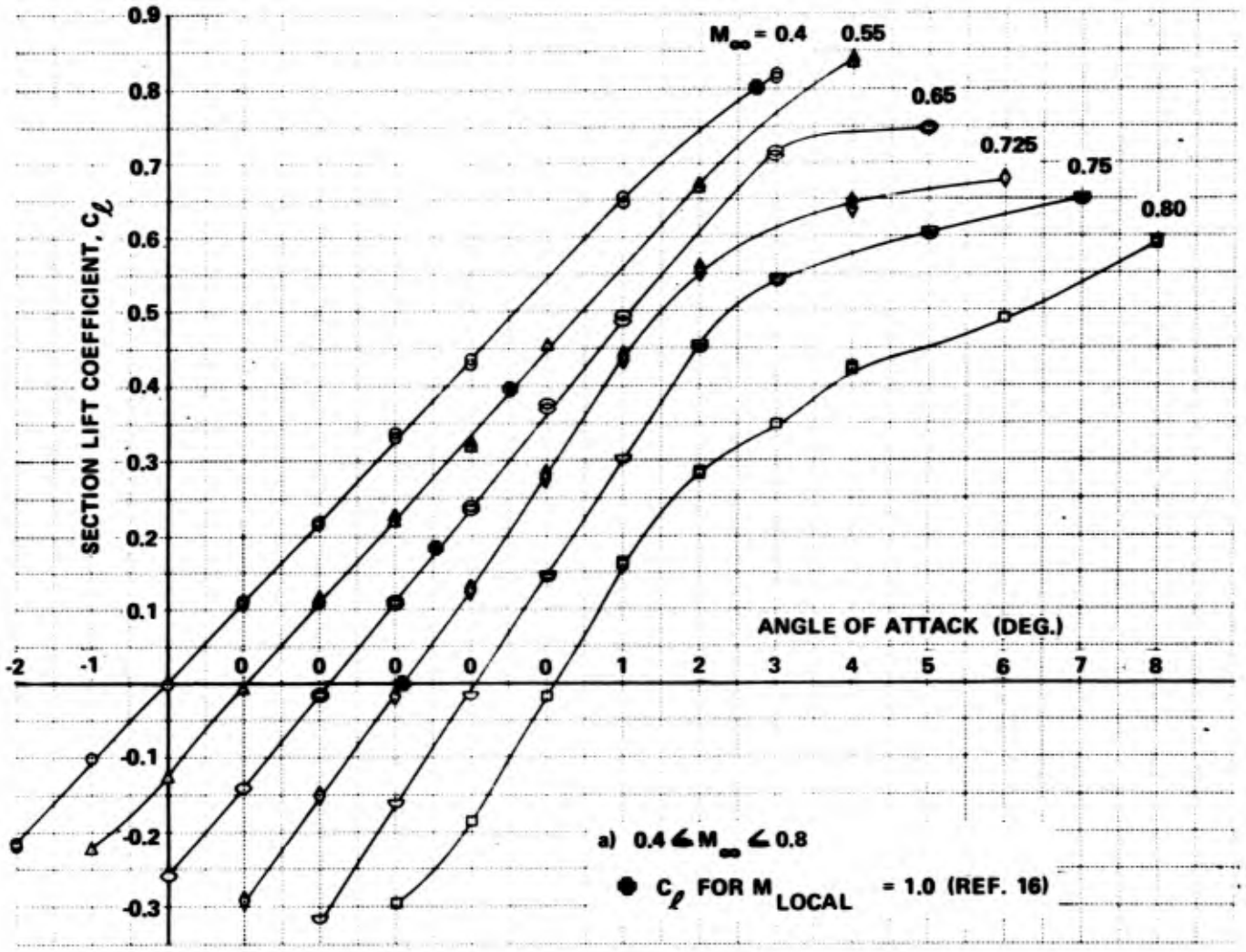

Figure 5 SECTION LIFT COEFFICIENT, Re = 10^6

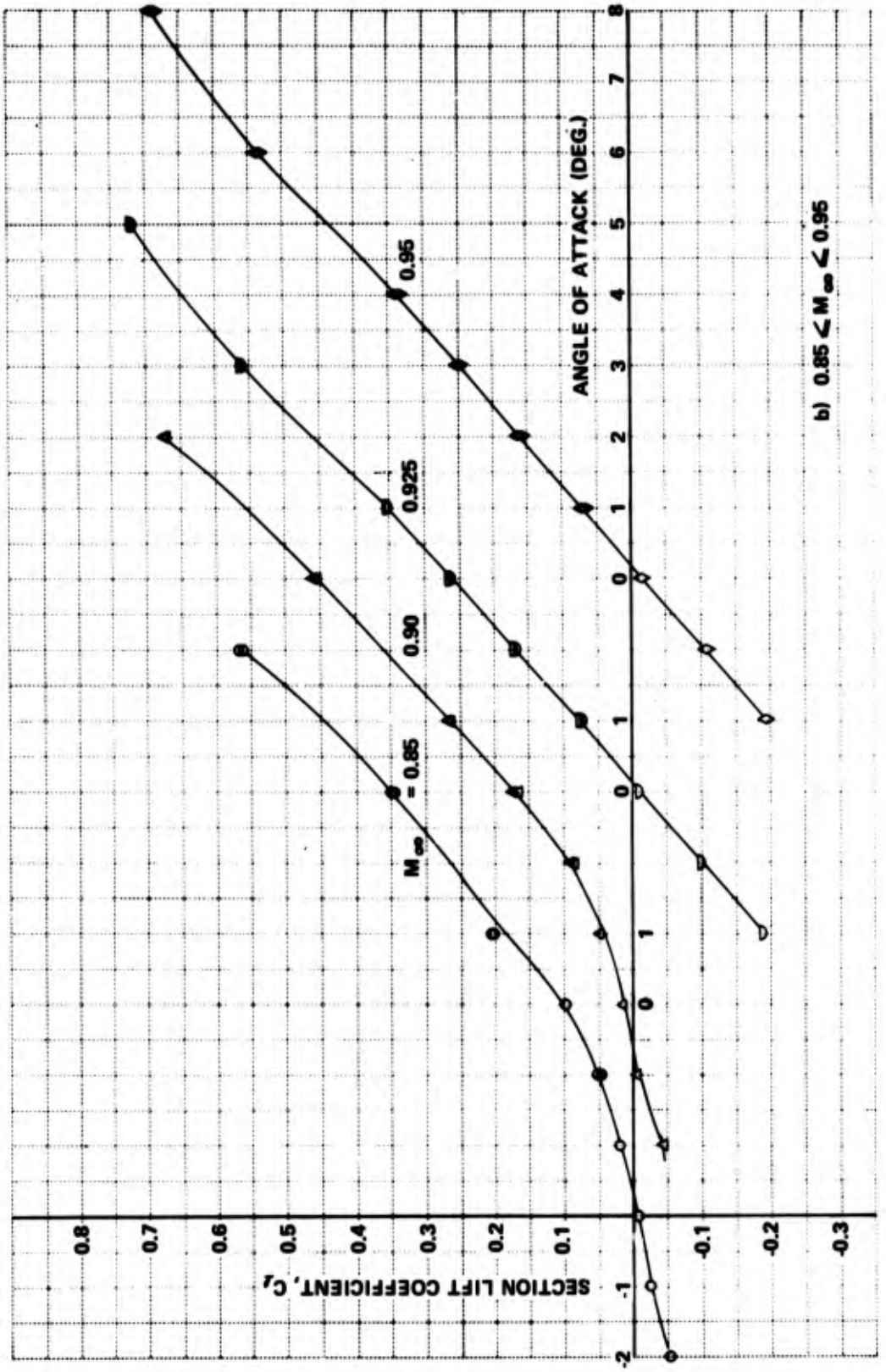

Figure 5 (Concluded) SECTION LIFT COEFFICIENT, $Re = 10^6$

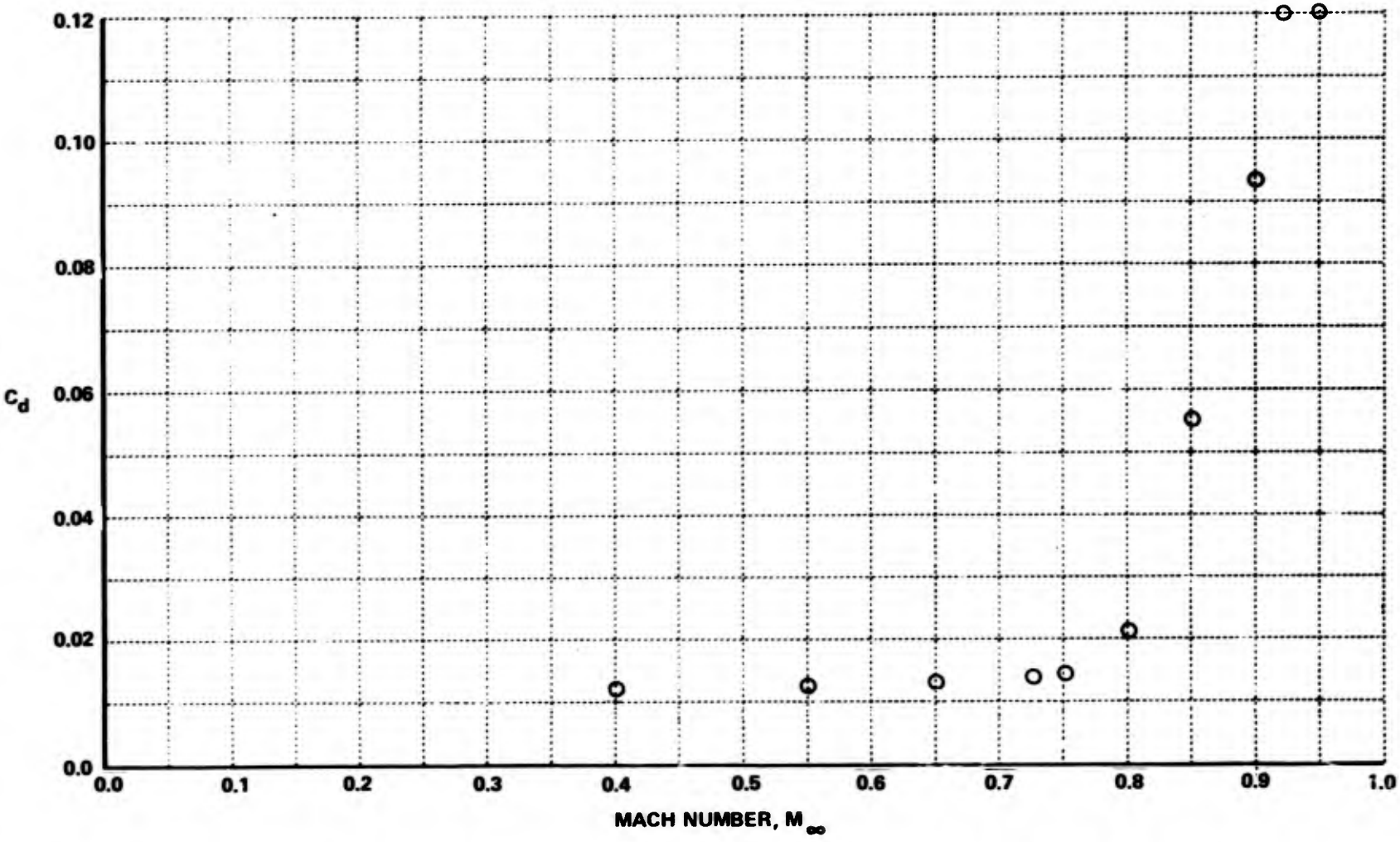

Figure 6 DRAG COEFFICIENT AT ZERO ANGLE OF ATTACK, Re = 10^6

expression for the drag, putting it in coefficient form, and then introducing the Prandtl-Glauert relation for the effects of compressibility on the inviscid disturbance velocity. The drag is obtained by integrating the viscous and pressure forces on the airfoil.

$$d = \oint \tau_w \cos\theta \, ds + \oint (p - p_\infty) \sin\theta \, ds \qquad (3)$$

where $\tau_w = \left(\mu \frac{\partial u}{\partial y}\right)_w$ is the local shear stress on the wall, θ is the local angle of the surface, and p and p_∞ are the local and ambient static pressures. The section drag coefficient is

$$C_d = \frac{2}{R_e} \oint \frac{U_e}{U_\infty} \left[\frac{\partial\left(\frac{U}{U_e}\right)}{\partial\left(\frac{y}{\delta}\right)}\right]_w \cos\theta \, \frac{ds}{\delta} + \oint C_p \sin\theta \, \frac{ds}{c} \qquad (4)$$

where U is the local inviscid velocity at the edge of the boundary layer. Using the linearized Prandtl-Glauert approximation, the above relation becomes

$$C_d = \frac{2}{R_e} \oint \left[1 + \frac{1}{\beta}\left(\frac{\Delta u}{U_\infty}\right)\right]\left[\frac{\partial\left(\frac{U}{U_e}\right)}{\partial\left(\frac{y}{\delta}\right)}\right]_w \cos\theta \, \frac{ds}{\delta} + \oint \frac{1}{\beta} C_{p_i} \sin\theta \, \frac{ds}{c} \qquad (5)$$

It is now assumed that (1) local flat plate similarity applies for the boundary layer on an airfoil, (2) the compressibility effects on the boundary layer profile and on the thickness are small, and (3) the airfoil is thin so that $\cos\theta \approx 1.0$. The first assumption is well established by the calculations of Squire and Young,[20] in which they applied flat plate data to account for thickness effects on frictional drag. The second was checked by applying the theory of Spalding and Chi[21] to estimate the change in local skin friction between $M_\infty = 0.725$ and $M_\infty = 1.0$, the worst conditions for the present data. This showed the local skin friction change by about 1% in this range.

Returning to Equation 5, the first term in the integration of the friction drag

$$\frac{2}{R_e} \oint [1] \left[\frac{\partial\left(\frac{U}{U_e}\right)}{\partial\left(\frac{y}{\delta}\right)}\right]_w \frac{ds}{\delta}$$

can be interpreted as the incompressible viscous drag on a flat plate at zero angle of attack. The remaining term is the increase in viscous drag due to the airfoil disturbance velocity. With this interpertation, Equation 5 can

then be cast into the following form

$$\beta\left[C_d - (C_{d_{FP}})_i\right] = \frac{2}{Re}\oint\left(\frac{\Delta u}{U_\infty}\right)_i\left[\frac{\partial\left(\frac{U}{U_e}\right)}{\partial\left(\frac{y}{\delta}\right)}\right]_w\frac{ds}{\delta} + \oint C_{p_i}\,\theta\,\frac{ds}{c} \quad (6)$$

This relation indicates that Prandtl-Glauert scaling applies to subcritical airfoil drag if the incompressible flat plate drag coefficient is subtracted from the compressible drag coefficient. It also indicates that this scaling applies even if there is flow separation since the pressure drag is included.

The scaling given by Equation 6 has been applied to the present data using Spalding-Chi theory[21] to estimate the incompressible flat plate drag. This estimate assumed that the boundary layer was fully turbulent from the leading edge, whereas actually the boundary layer was laminar over the first 10% of the airfoil chord. This assumption introduces an uncertainty of about 5% in the incompressible flat plate drag. The scaled and unscaled data are plotted on an expanded scale in Fig. 7 for angles of attack 0°, 2°, and 3°. The unscaled data show significant Mach number effects and the scaled data show they are removed effectively by this application of Prandtl-Glauert scaling.

The drag data at constant lift coefficient are plotted versus Mach number in Fig. 8. It can be seen that the drag rise begins at Mach numbers somewhat higher than the theoretical critical Mach number.

Pitching Moment

The pitching moment coefficient data at constant lift coefficient are plotted versus Mach number in Fig. 9. An important point to notice is the nosedown moment occurring at $M_\infty = 0.85$ for lift coefficients of 0.1 to 0.4. It was found in the pressure distribution data that a shift in the position of the shock waves on the airfoil accompanied by a redistribution of the lift over the airfoil caused the noticeable change in the moment.

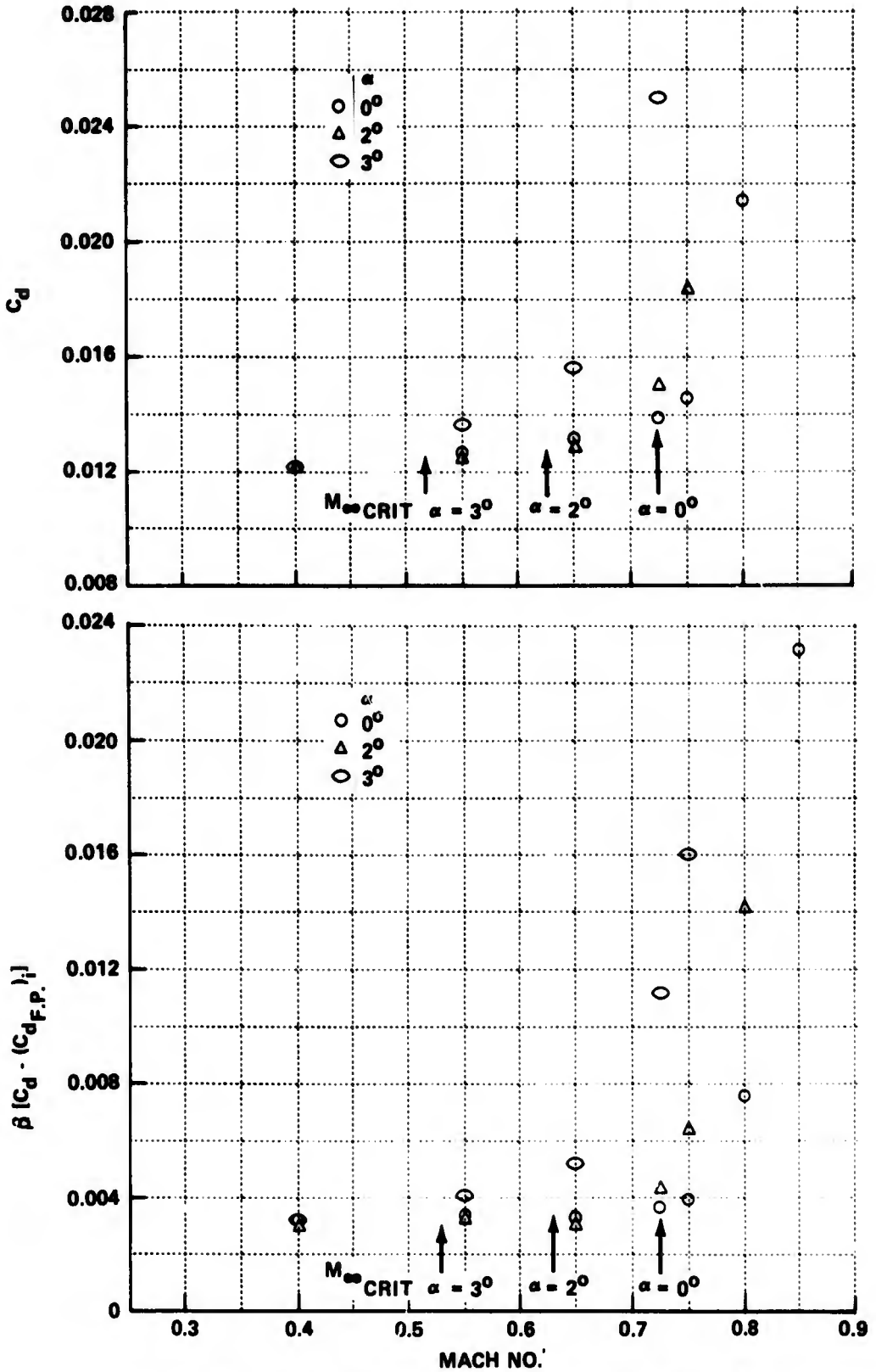

Figure 7 AIRFOIL PROFILE DRAG Re = 10^6

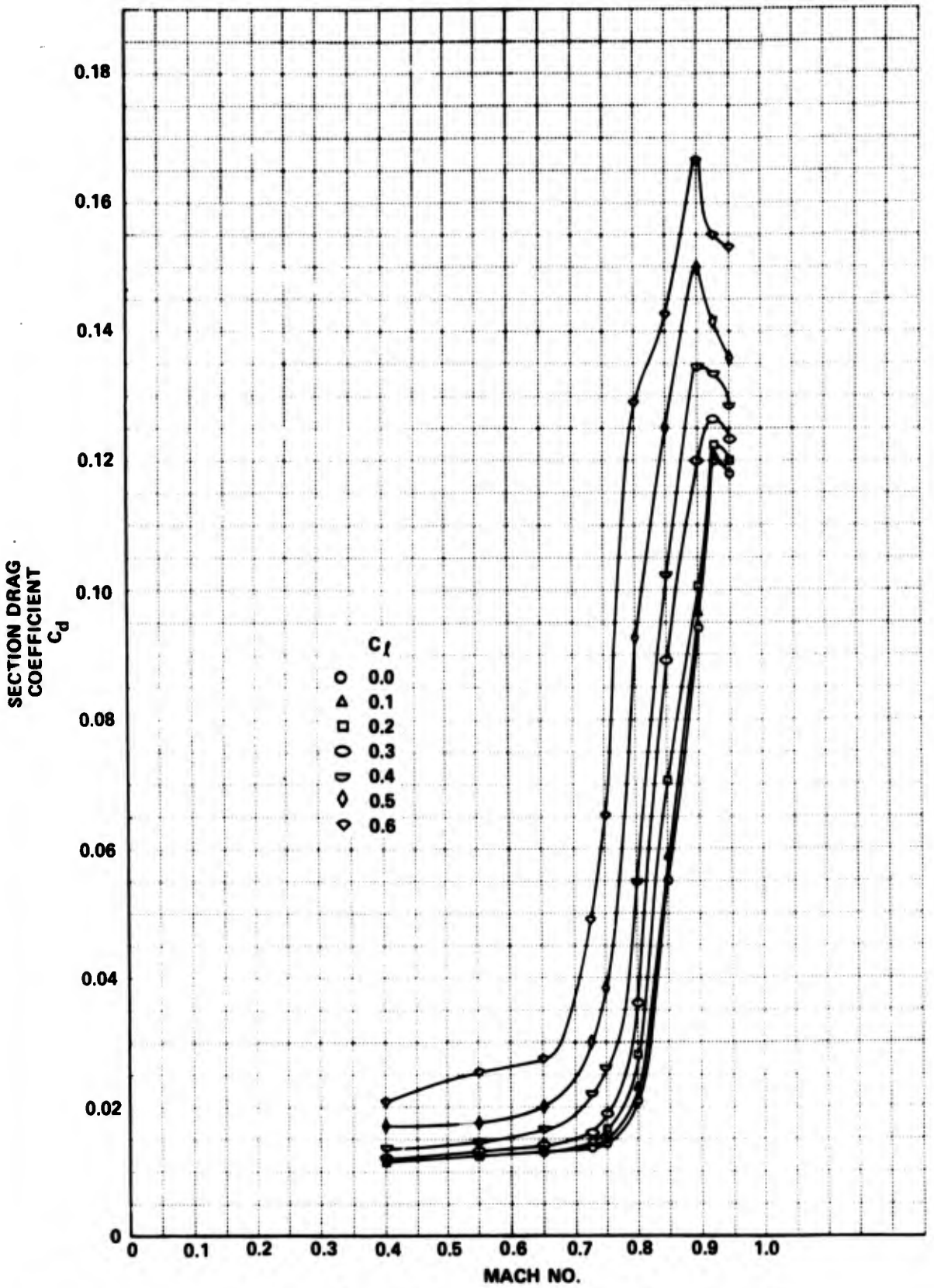

Figure 8 AIRFOIL DRAG COEFFICIENT, Re = 10^6

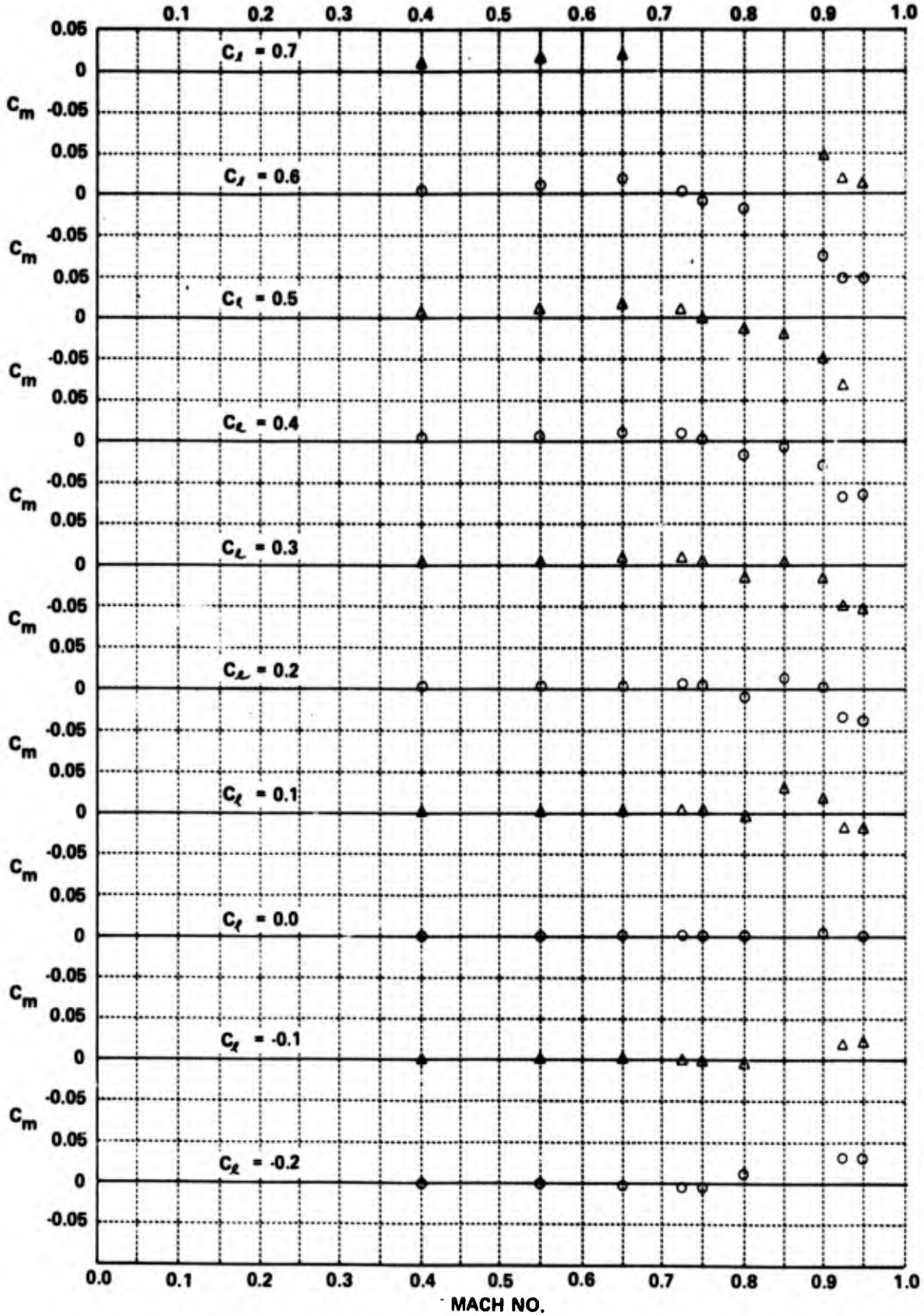

Figure 9 AIRFOIL PITCHING MOMENT COEFFICIENT, Re = 10^6

Pressure Distributions

The pressure data obtained on the airfoil upper surface at zero angle of attack are presented in Figs. 10 to 14. These data have been reduced to an incompressible value using both Prandtl-Glauert and von Kármán-Tsien scaling, and are compared with incompressible theory taken from Ref. 16. Included in these figures is a tabulation of the critical pressure coefficient, $\beta C_{p_{CRIT}}$, corresponding to local sonic conditions. It can be seen that for subcritical ambient Mach numbers, Fig. 10, the Prandtl-Glauert scaling collapses the data reasonably well except in the vicinity of the leading edge. Some of the scatter near the leading edge stems from the small flow angularity producing a small negative lift on the airfoil. The scaled data in Fig. 10 have been corrected for the small lift effect using the linear incompressible theory of Ref. 16 and are shown in Fig. 11. It can be seen that this correction reduces the scatter somewhat near the leading edge, and that the data in this region tend to fall below the incompressible theory.

The subcritical pressure data have also been scaled using the von Kármán-Tsien scaling parameter, $C_{p_i} = \dfrac{\beta C_p}{1 - \dfrac{M_\infty^2}{1+\beta}\dfrac{C_p}{2}}$, and are compared with incompressible theory in Figs. 12 and 13. Figure 12 shows the data at zero geometric angle of attack, and comparing it with Fig. 10, it can be seen that the von Kármán-Tsien scaling produces a slightly better correlation. Again, some of the scatter in the vicinity of the leading edge can be attributed to flow anglularity and the small negative lift on the airfoil. The scaled data in Fig. 12 have been corrected to zero lift, again using incompressible linear theory,[16] and are compared with this theory in Fig. 13. It can be seen that the correction to zero lift produces a better correlation among different Mach numbers and produces improved agreement between theory and experiment. The data, however, fall below the incompressible theory, especially on the forward 25% of the airfoil chord. These discrepancies might be attributed to machining tolerances in fabricating the airfoil, but it should be noted that the tolerances were no greater than $\pm$ 0.001 inches.

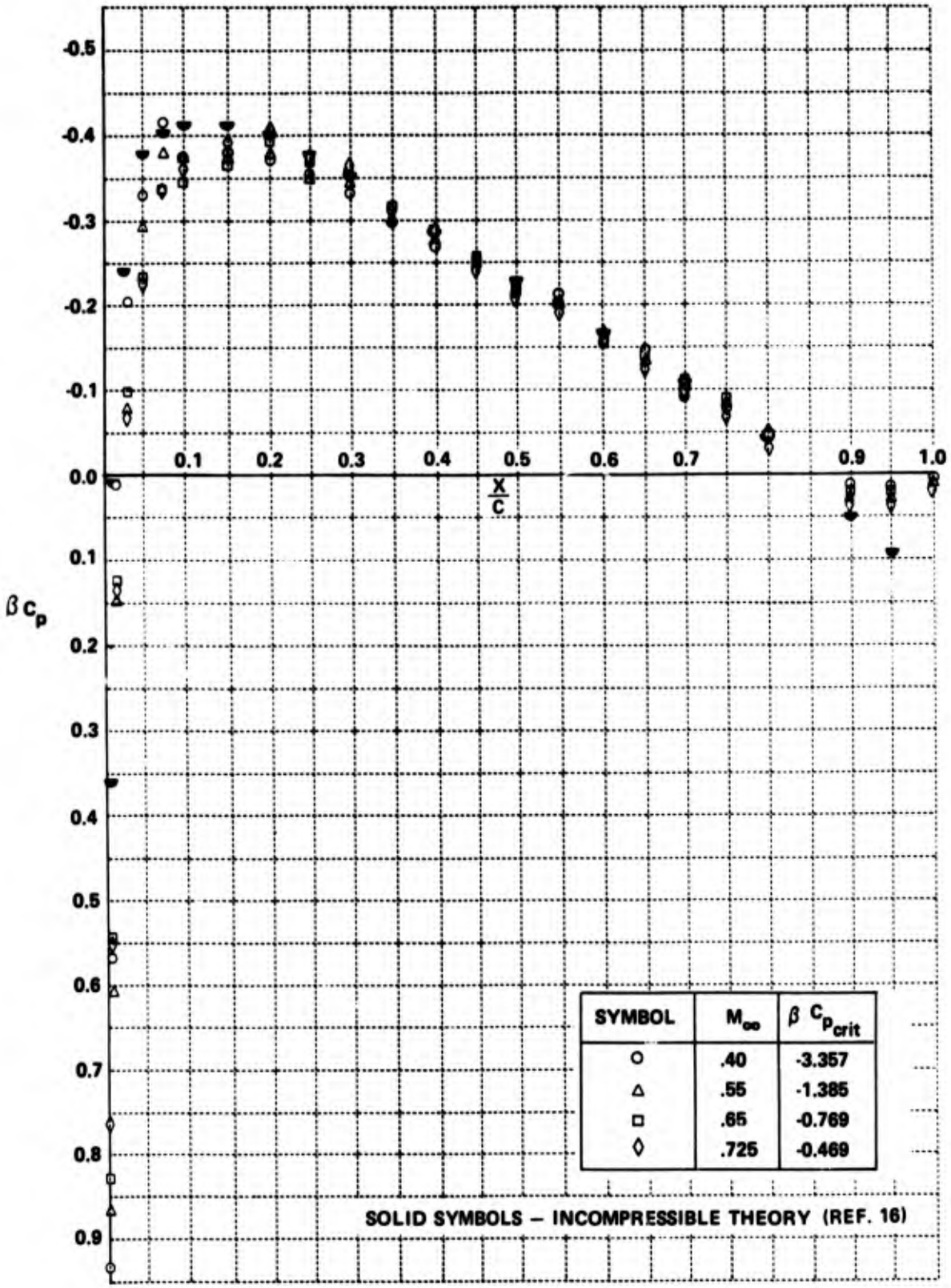

Figure 10 PRANDTL-GLAUERT SCALING OF THE UPPER SURFACE PRESSURE DISTRIBUTION, $\alpha = 0^{o}$

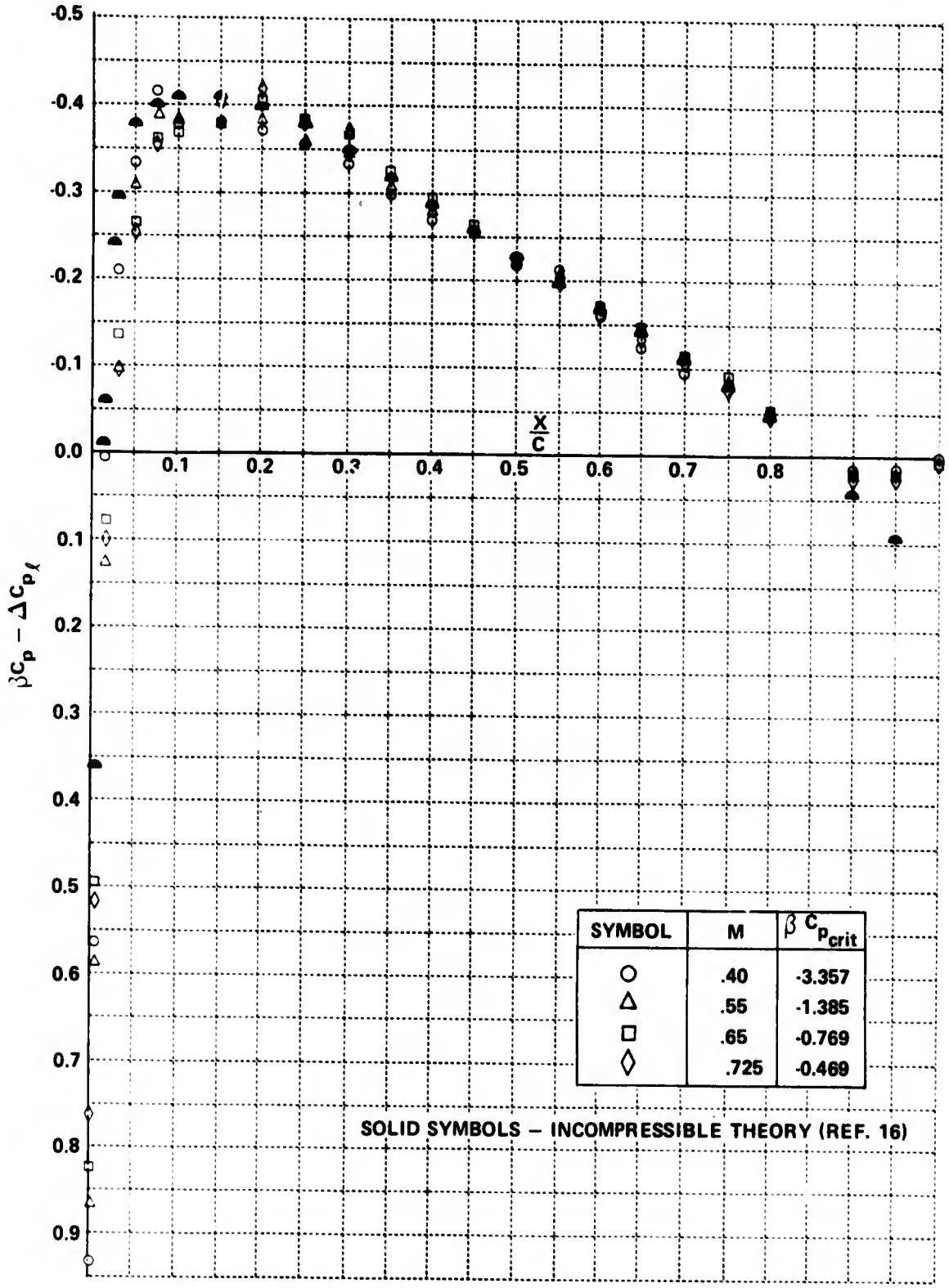

Figure 11 PRANDTL-GLAUERT SCALING OF THE UPPER SURFACE PRESSURE DISTRIBUTION, $C_\ell = 0$

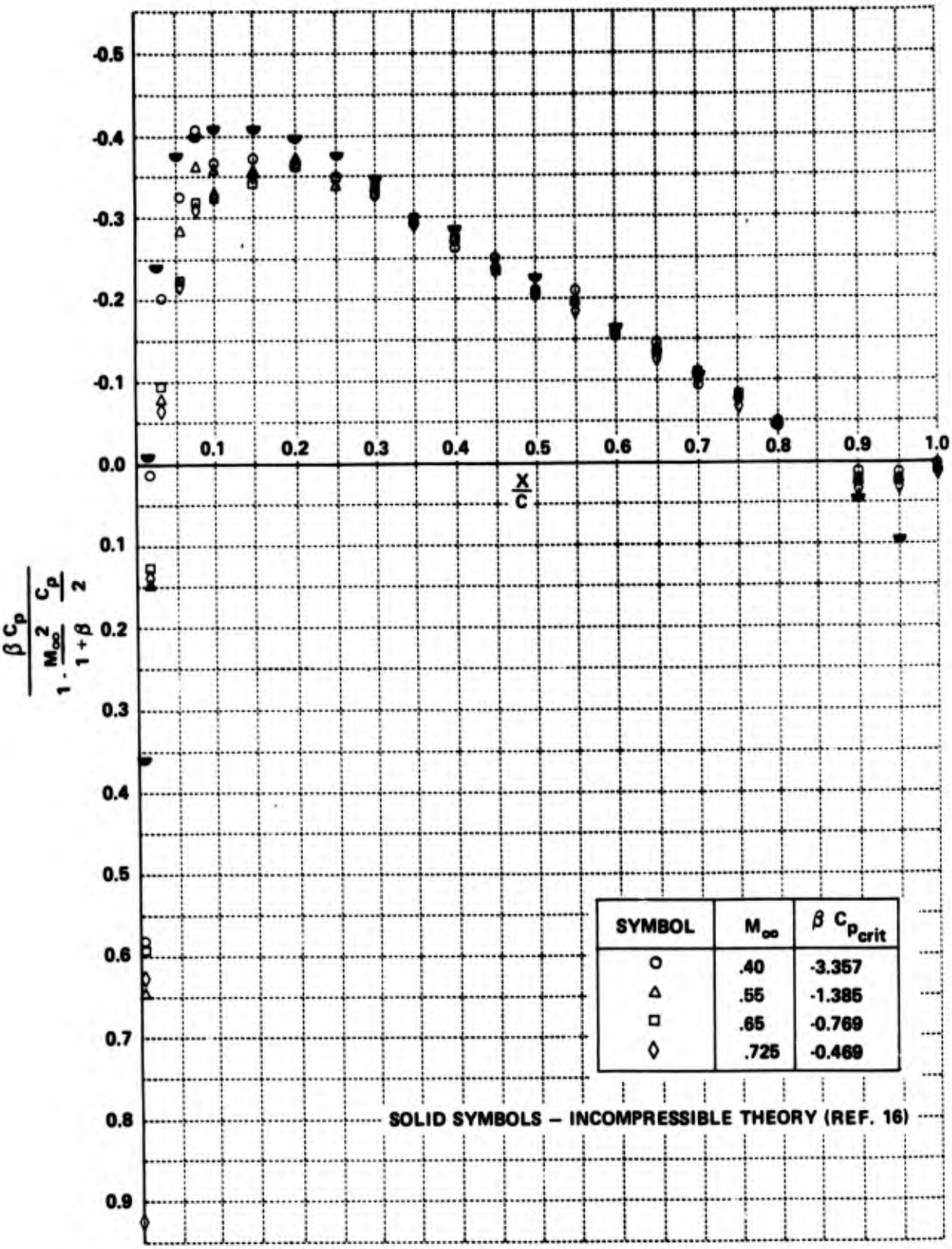

Figure 12 VON KÁRMÁN-TSIEN SCALING OF THE UPPER SURFACE PRESSURE DISTRIBUTION, $\alpha = 0^o$

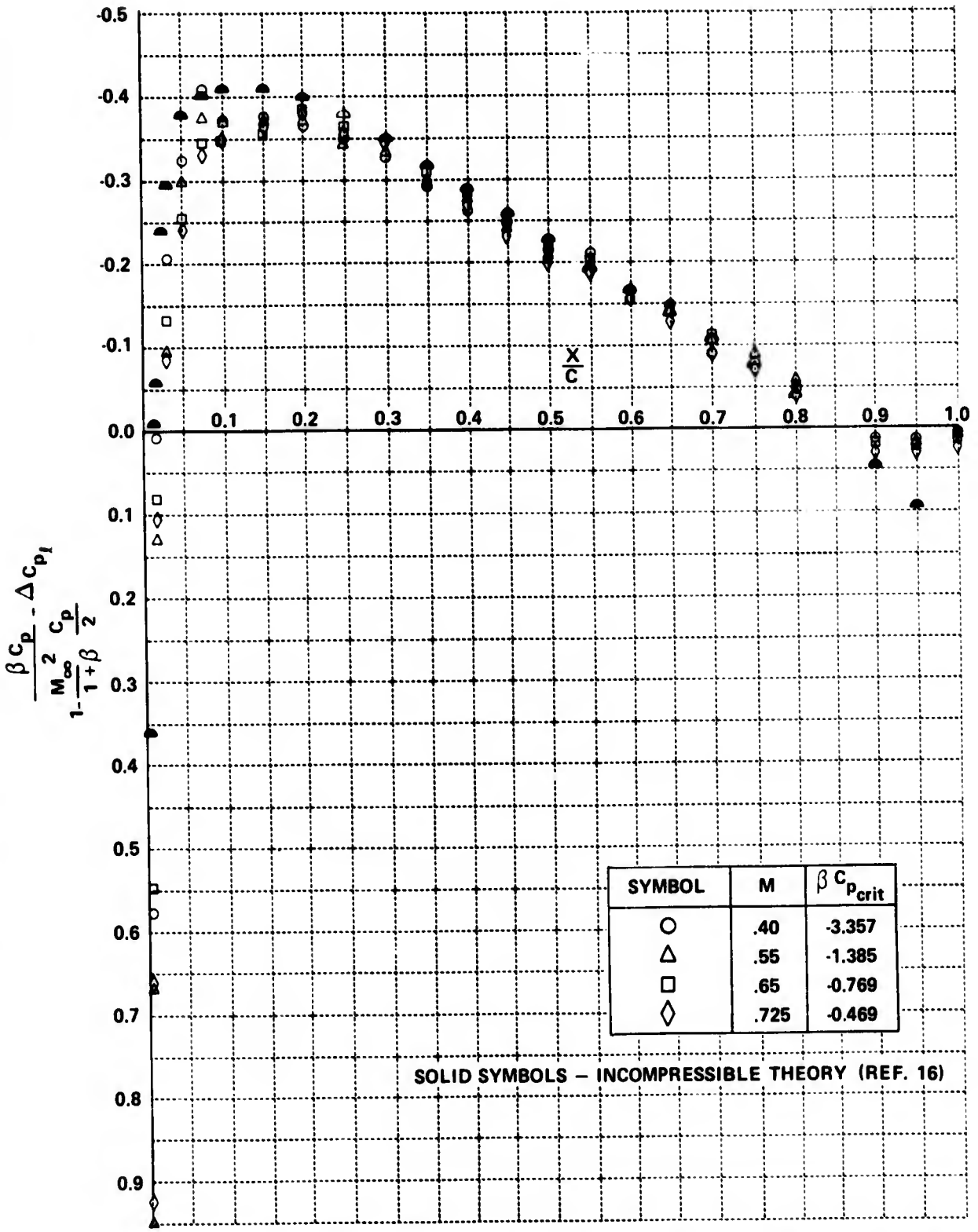

Figure 13 VON KÁRMÁN-TSIEN SCALING OF THE UPPER SURFACE PRESSURE DISTRIBUTION, $C_\ell = 0$

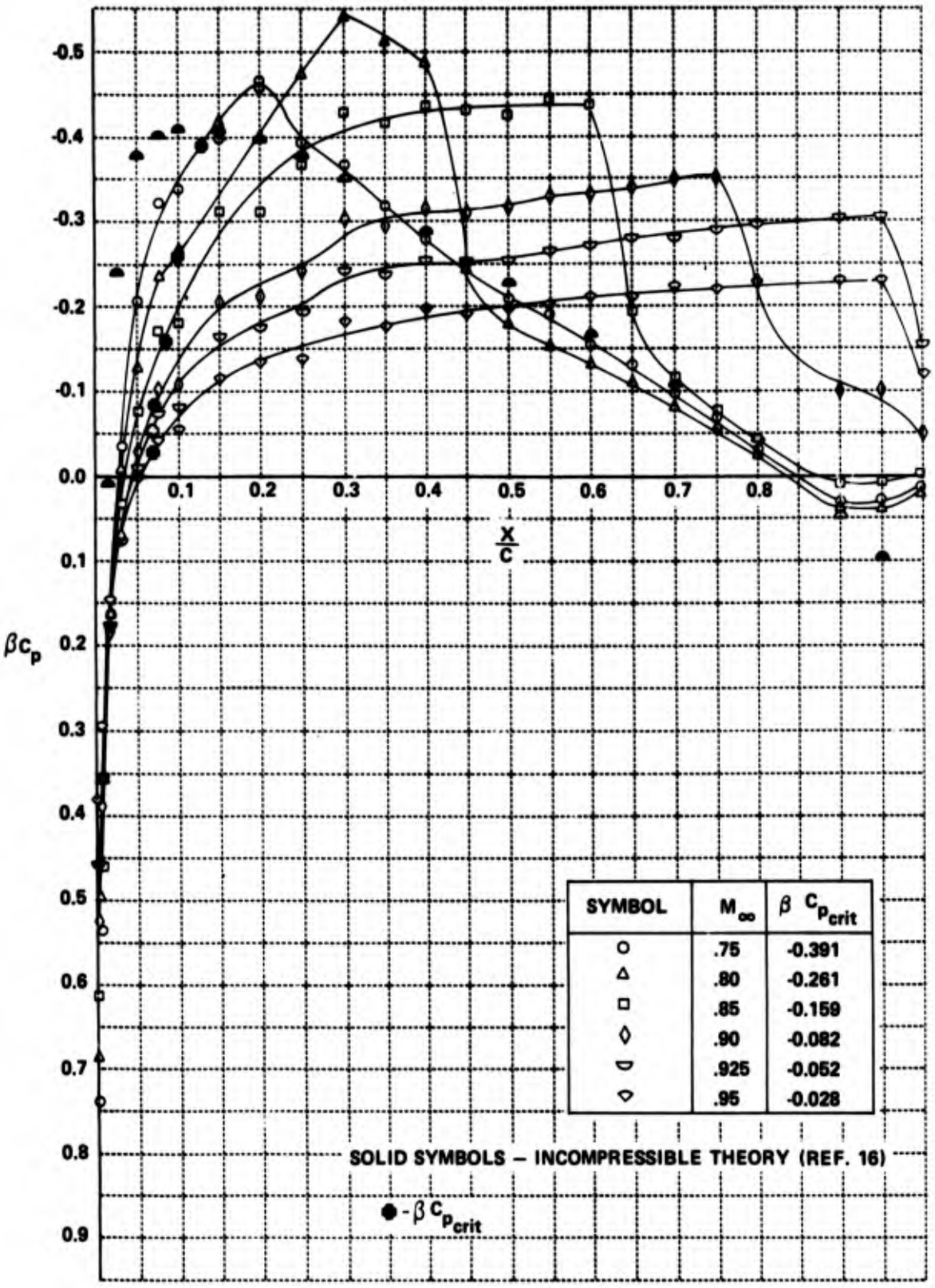

Figure 14 PRANDTL-GLAUERT SCALING OF THE SUPERCRITICAL PRESSURE DISTRIBUTION, α = 0

A final point to note in connection with Fig. 10 to 13 is that the theoretical critical Mach number for this airfoil[16] is 0.725, and the corresponding value of βC_p for sonic flow is -0.469. The maximum value of βC_p measured in these experiments is about -0.41 and is substantially below the theoretical critical value. Therefore, the critical Mach number seems to be somewhat higher than 0.725.

The data obtained at supercritical Mach numbers and zero angle of attack have been scaled with the Prandtl-Glauert parameter and are compared with incompressible theory in Fig. 14. The critical values of the scaled pressure coefficient, $\beta C_{p_{CRIT}}$, are tabulated in the figure and are indicated on each of the faired curves. The data obtained at $M_\infty = 0.75$ show that the airfoil is supercritical at this Mach number with a peak pressure coefficient corresponding to a local Mach number of about 1.05. There is evidence of either a weak shock wave or a nearly isentropic compression in the region $\frac{x}{c} = 0.20$ to 0.25 because the pressure coefficient at $\frac{x}{c} = 0.25$ indicates a local Mach number of about 1.0. The pressure distribution downstream of the recompression zone is in reasonable agreement with incompressible theory. Similar comments apply to the data for $M_\infty = 0.80$ and 0.85. The data at $M_\infty = 0.90$ show that the flowfield is almost entirely supersonic, and at the two highest Mach numbers it is entirely supersonic.

In Fig. 15 two supercritical pressure distributions are plotted for an angle of attack of one degree. Scaled pressure coefficients for both the upper and lower surfaces of the airfoil are plotted, and the flagged symbols are for the lower surface. The position of the shock on the upper surface is well defined by the rapid change in the pressure at $\frac{x}{c} \approx 0.275$ for Mach number 0.75 and at $\frac{x}{c} \approx 0.525$ for Mach number 0.80. Oil flow photographs taken of the upper surface of the airfoil confirm these shock positions, Figs. 16 and 17, and are typical of the agreement, regarding shock position, between the oil flow photographs and the surface pressure distributions. Apparently the pressure rise through the shock wave acts as a barrier to the oil flow and causes it to accumulate at the shock wave.

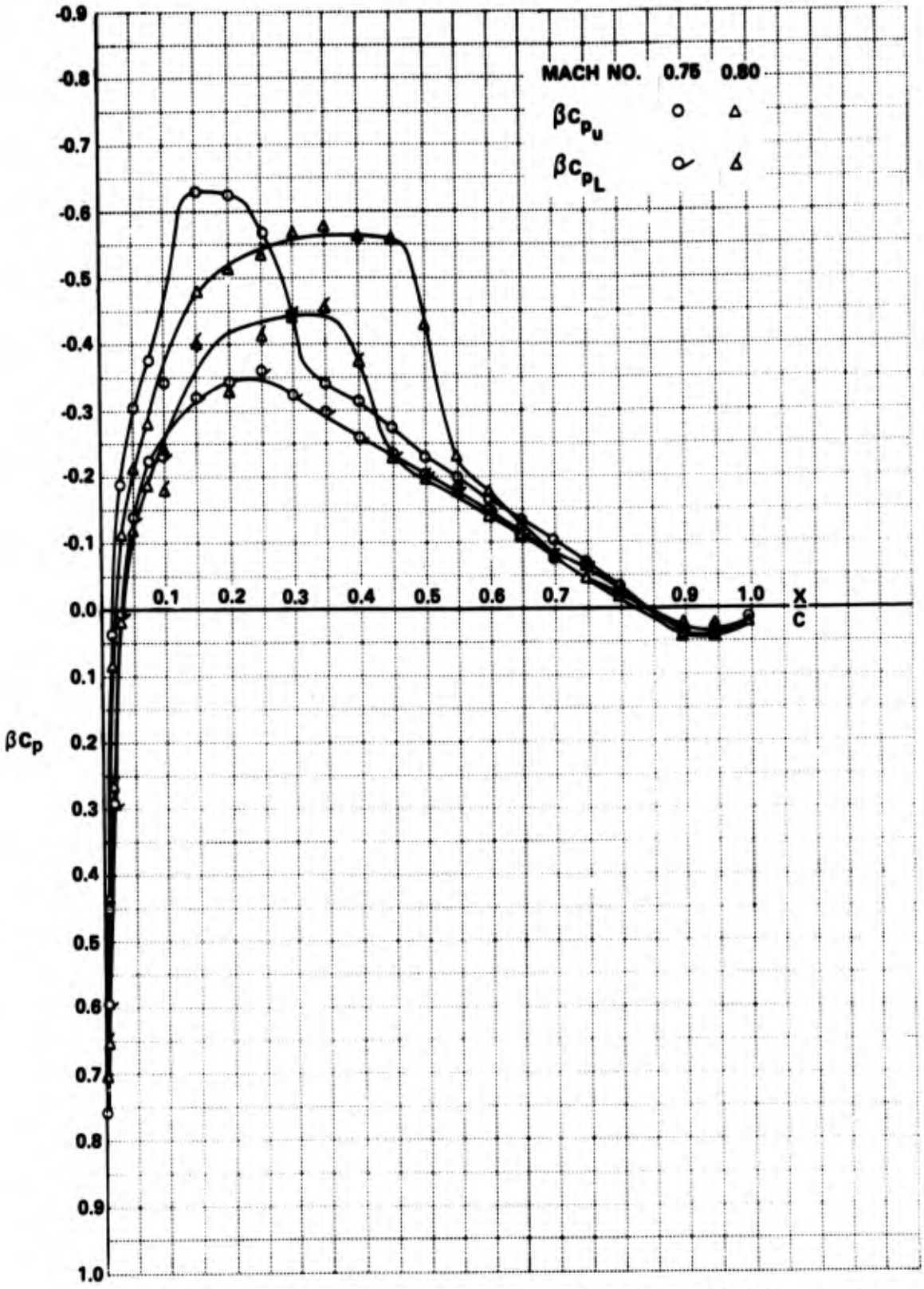

Figure 15 SUPERCRITICAL PRESSURE DISTRIBUTIONS $\alpha = 1^o$

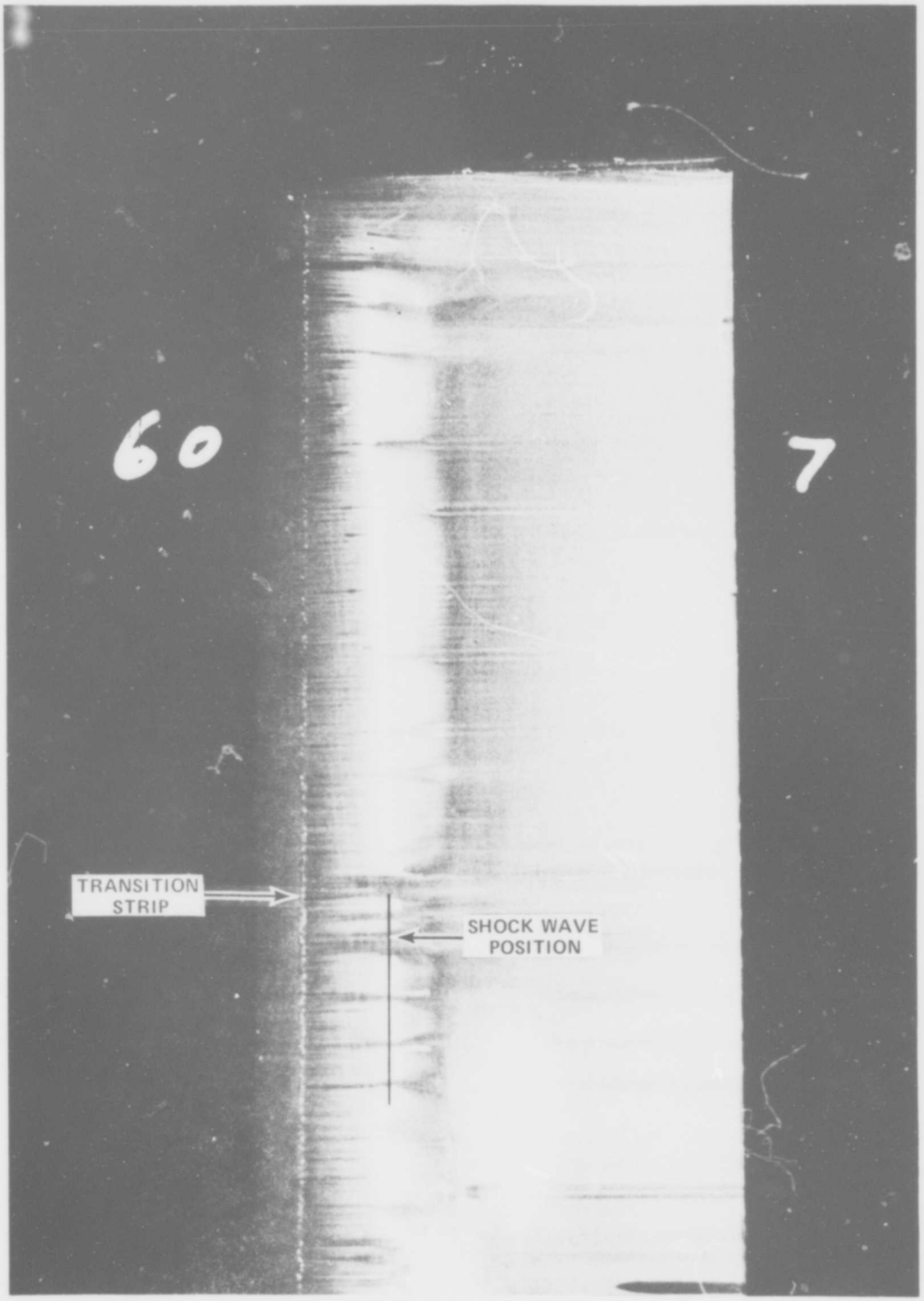

Figure 16 OIL FLOW PHOTOGRAPH OF THE AIRFOIL UPPER SURFACE
$M_\infty = 0.75 \quad \alpha = 1^o$

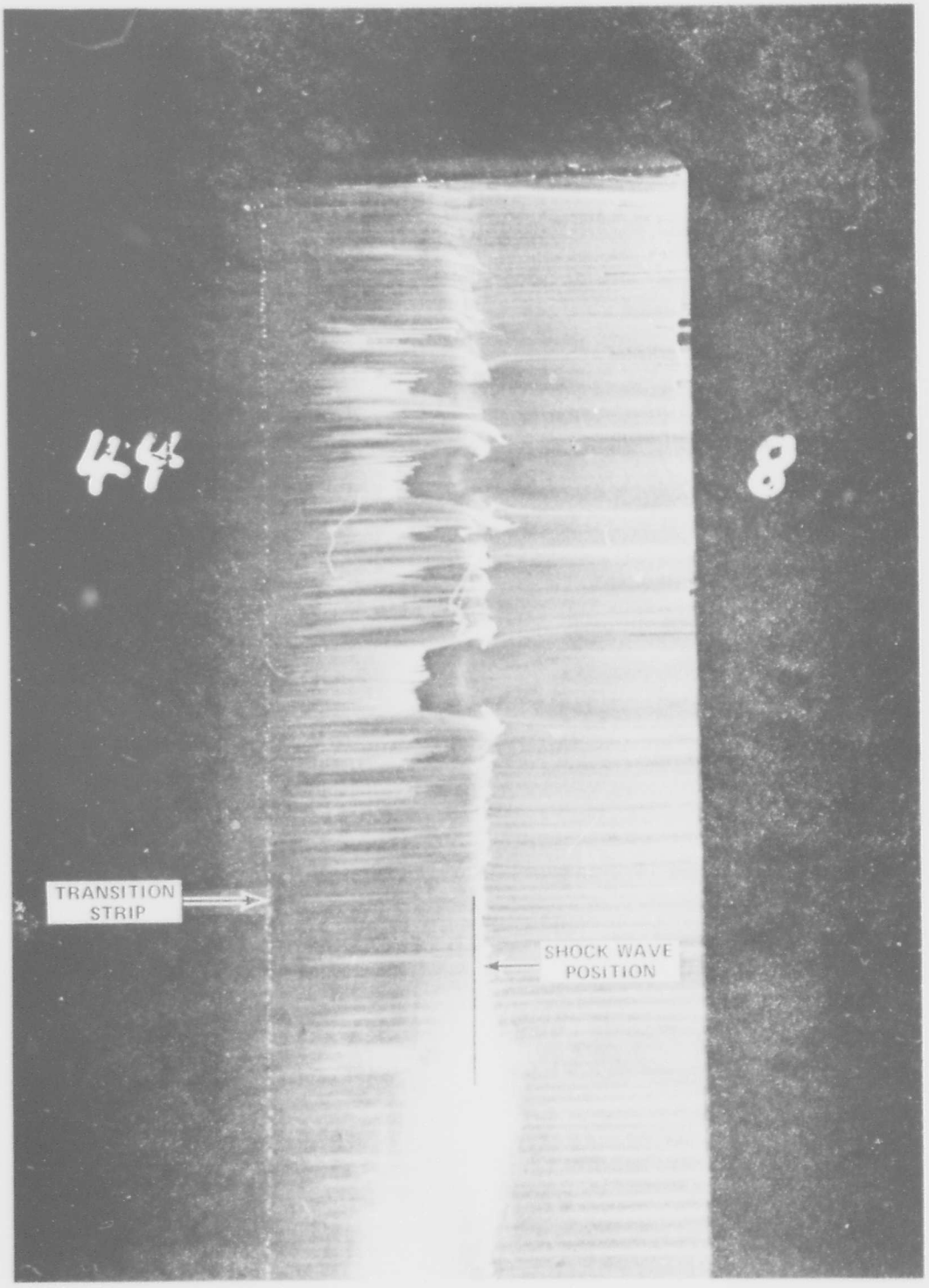

Figure 17 OIL FLOW PHOTOGRAPH OF THE AIRFOIL UPPER SURFACE
$M_\infty = 0.80$ $\alpha = 1^o$

In the discussion of the airfoil lift, it was noted that at small angles of attack for a Mach number of 0.85, there was a noticeable decrease in the lift curve slope. The moment coefficient also changed markedly at a Mach number of 0.85 for small angles. Both the loss of lift and the large positive increase in pitching moment coefficient can be detected in the pressure distribution presented in Fig. 18. The airfoil pressure distribution at a geometric angle of attack of 1° and a Mach number of 0.85 indicates a relative increase in the pressure over a large portion of the lower surface of the airfoil. This in turn results in a general decrease in the overall lift at this Mach number. It can also be seen that, unlike other Mach numbers, there is a net downward loading at $x/c \approx 0.5$ to 0.65 that results in the considerable noseup moment that is experienced at this Mach number.

Comparisons With Other Data

As noted earlier, one reason for using the 0012 section in the present research was because there is a body of current theoretical and experimental data available for the airfoil at transonic speeds. Some of the present pressure data are compared with the exact solution given by Sells[22] and as reported by Lock[4] in Figs. 19 and 20. The experimental data in Fig. 19 nominally are for $\alpha = 0°$ and are the average of the upper and lower surface pressures obtained at an angle of attack of -0.10°. It is noted that rigorously this averaging does not reproduce the result for zero lift, but the maximum error in the present case is about 5×10^{-3}%. The comparison in Fig. 19 shows that the theory and experiment in general are in good agreement except in the region $0.10 \leq x/c \leq 0.25$ where the data is less than theory by a maximum of about 5%.

A similar comparison is made in Fig. 20 between the theory reported by Lock[4] and the present data at $\alpha \approx 2°$. It should be noted that the present data were obtained at a slightly higher Mach number and a slightly lower angle of attack. The effect of the higher Mach number is to increase the experimental pressure coefficients by about 2.2% and the effect of the

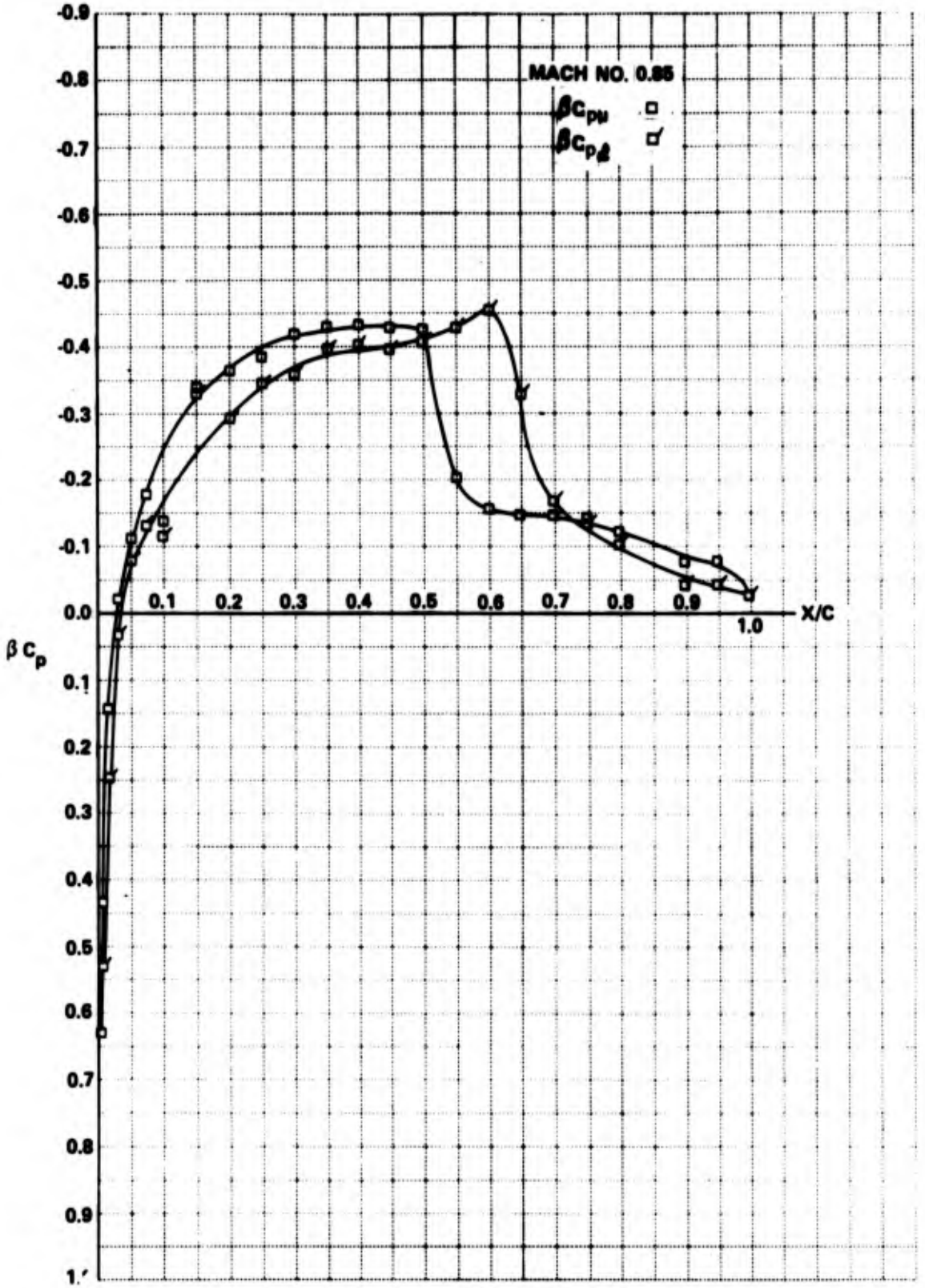

Figure 18 SUPERCRITICAL PRESSURE DISTRIBUTIONS $\alpha = 1^o$

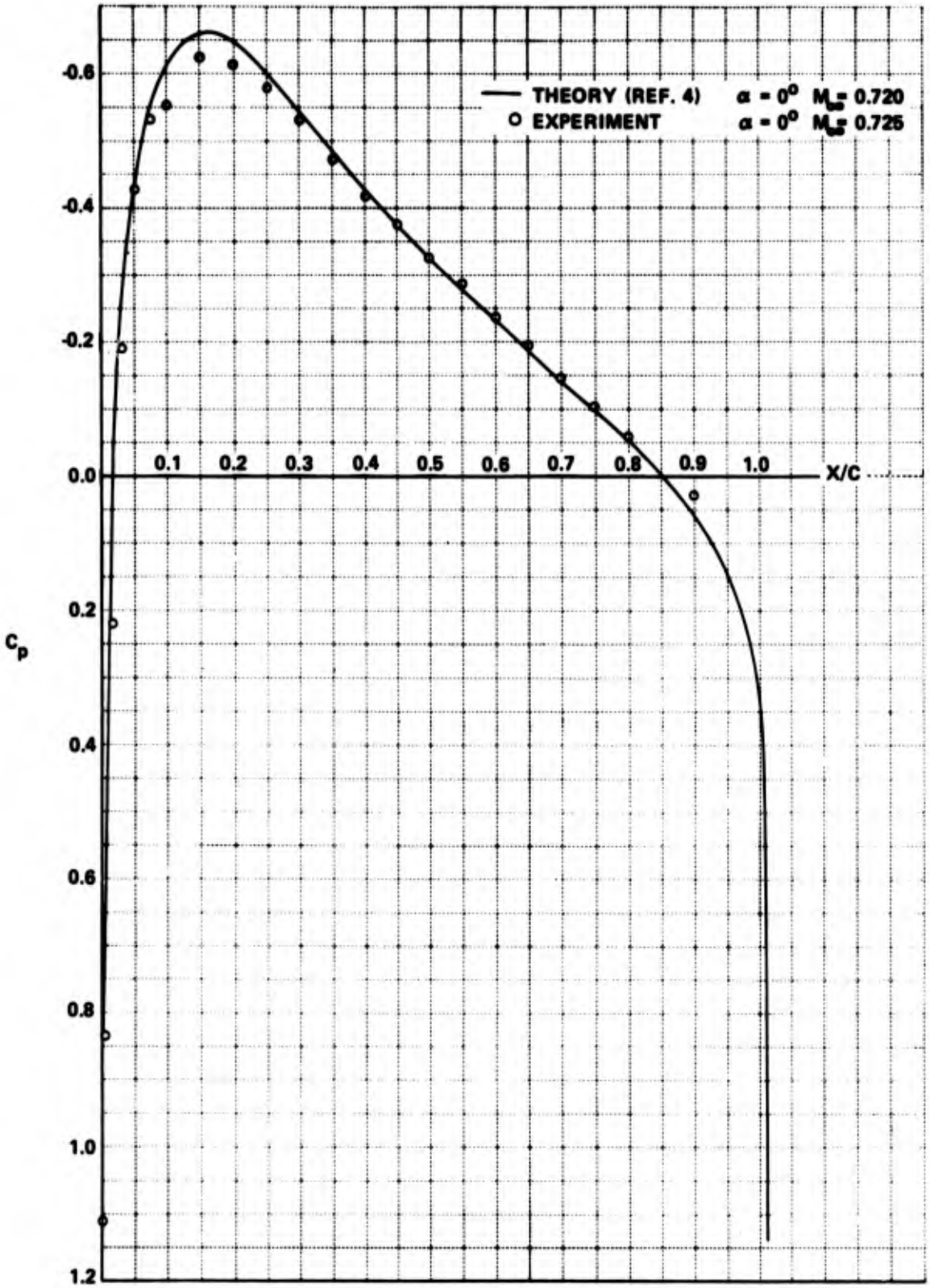

Figure 19 COMPARISON BETWEEN THEORY AND EXPERIMENT

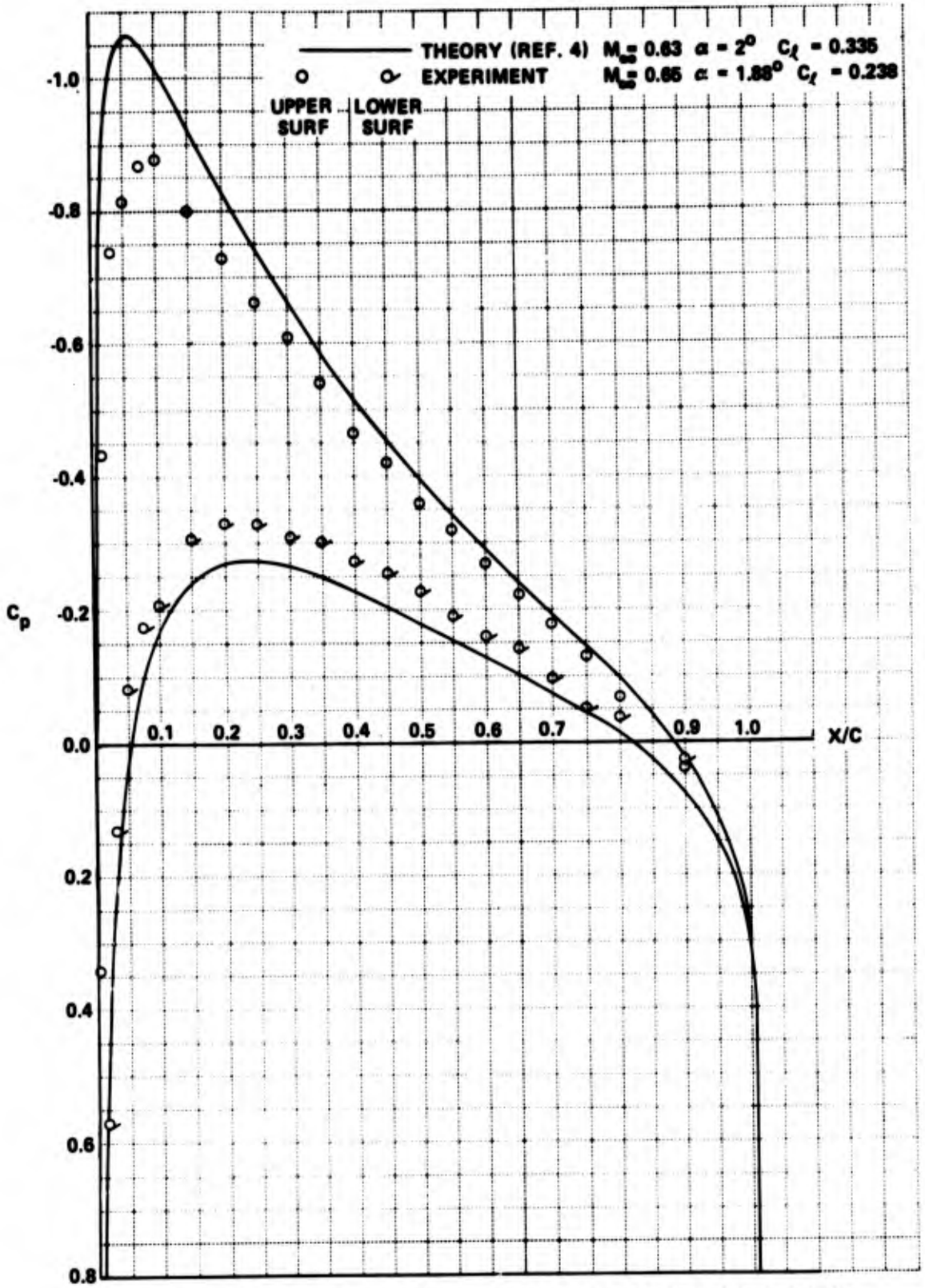

Figure 20 COMPARISON BETWEEN THEORY AND EXPERIMENT

lower angle of attack is to decrease the experimental pressure coefficients by about 2.3%. Consequently, the two effects nearly cancel and the comparison in Fig. 20 is reasonably valid. It can be seen in Fig. 20 that the maximum difference between theory and experiment is about 20%. The theory predicts a lift coefficient about 40% higher than that measured in the present experiments. Part of this discrepancy probably can be attributed to the fact that the theory is inviscid. The viscous correction given by Spence[17] would account for a 14% difference in lift coefficient, but of course Spence's correction may not be valid in this range. The source of the remaining discrepancy is not clear.

Osborne is conducting transonic two-dimensional experiments with an NACA 0012 section at the RAE in Teddington and made his provisional data available to the authors.[5] His research is being performed in a 36-in. by 14-in. test section with two slotted and two solid walls. The initial experiments were made with airfoils of 5-in. and 10-in. chord lengths, and the slot geometry was varied to arrive at interference-free conditions, as indicated by agreement between the two sets of airfoil pressure data. His data were obtained at Reynolds numbers of about 3×10^6 and with transition fixed by grit at the leading edge or at 15% of the chord. Comparisons are made with Osborne's data in Fig. 21 through 23.

Data obtained at supercritical conditions, zero angle of attack and a Mach number of 0.8, are presented in Fig. 21, and generally are in good agreement over the entire chord length. There is a slight difference in Mach number for the two experiments which could account for the small discrepancies between the two sets of data. The one discrepancy that should be noted is in the position of the shock wave; it is 4% of the chord further aft in the present experiment. This discrepancy is probably due to the differences in Mach number since the shock position is quite sensitive to Mach number changes in this range of Mach numbers.

The pressure data obtained at a nominal angle of attack of 2° and at a subcritical Mach number are compared with Osborne's data in Fig. 22.

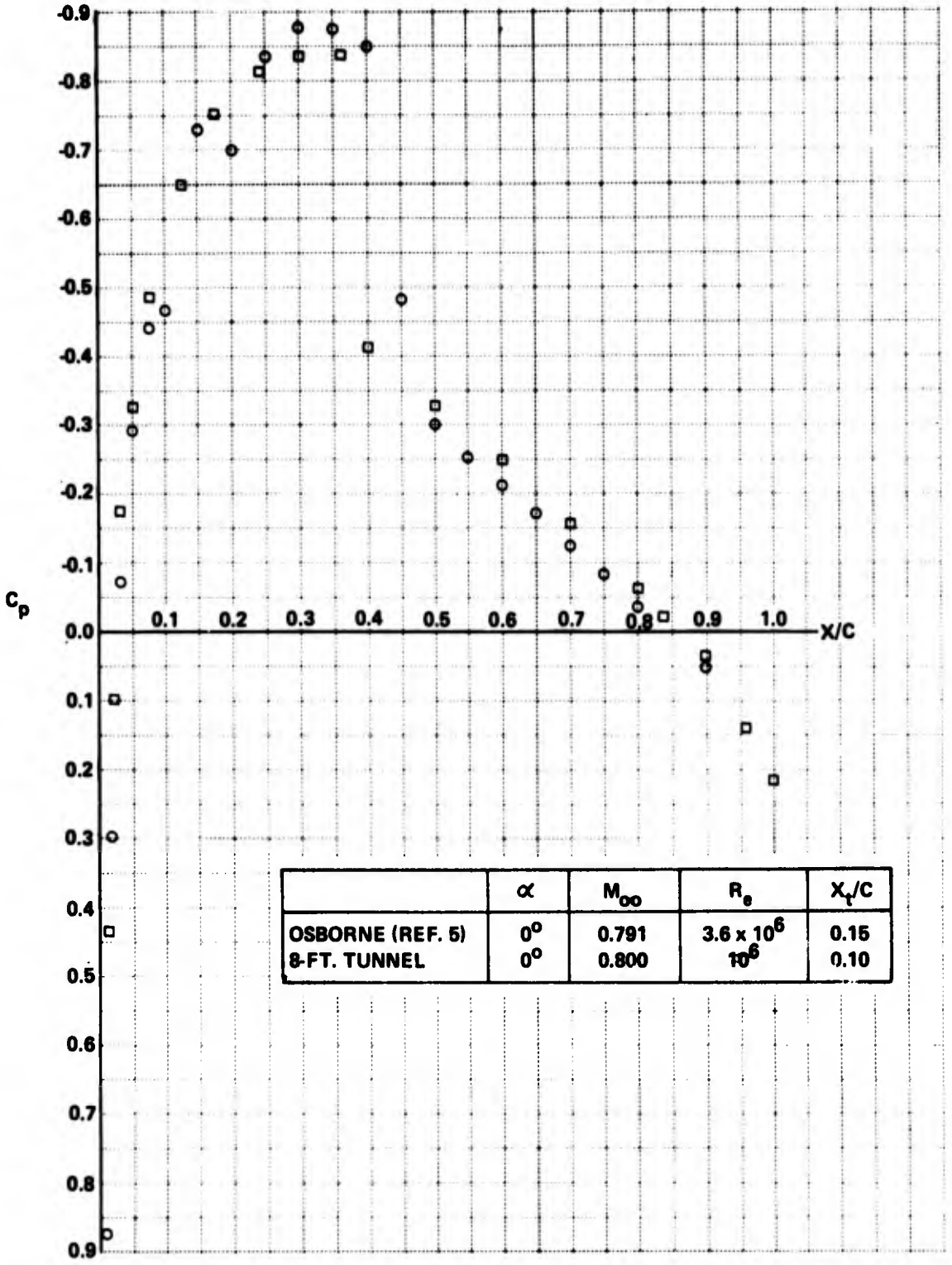

Figure 21 COMPARISON WITH OTHER EXPERIMENTAL DATA

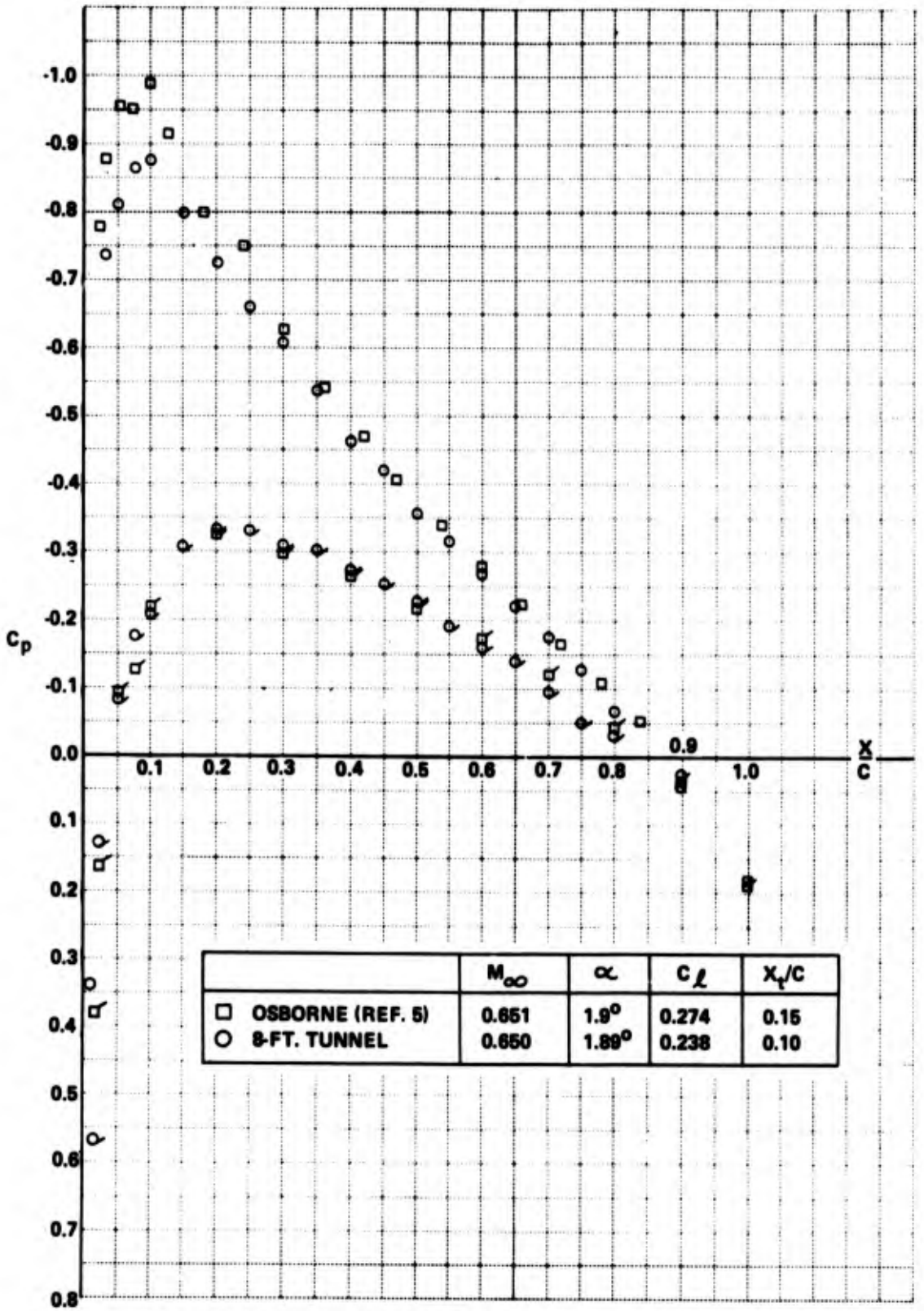

Figure 22 COMPARISON WITH OTHER EXPERIMENTAL DATA

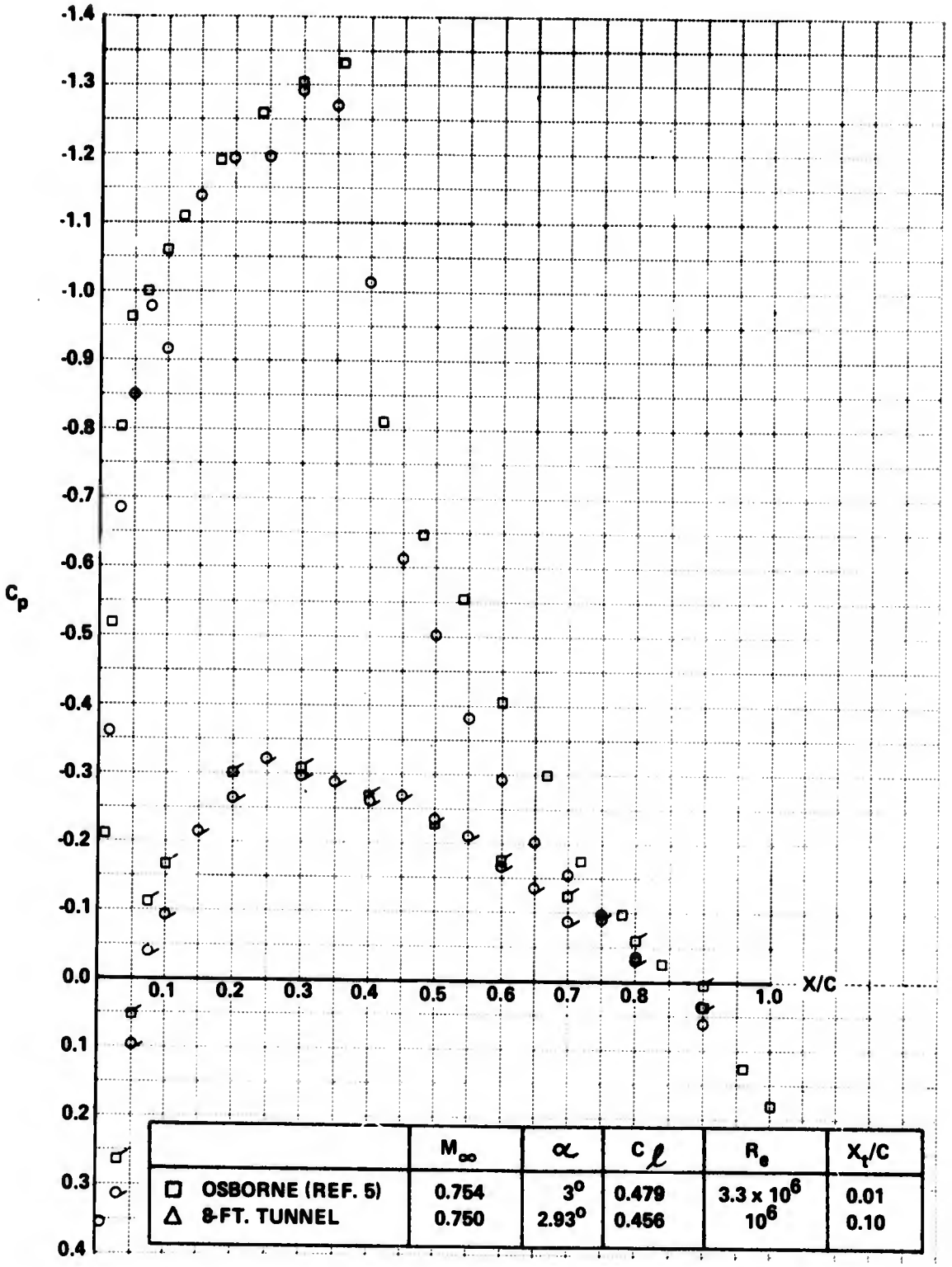

Figure 23 COMPARISON WITH OTHER EXPERIMENTAL DATA

It can be seen that the data for the lower surface are good agreement, but the present data on the upper surface fall substantially below Osborne's data. It should be noted that both the angle of attack and the lift coefficient given by Osborne have been corrected for blockage in an approximate manner, and the nominal angle of attack quoted is 2.0°. If the actual angle of attack in his experiments were 2.0°, it would account partially for the differences in lift coefficient and the differences in the pressure distribution.

Pressure data obtained at supercritical conditions, an angle of attack of 3° and a Mach number of 0.75, are compared with Osborne's data in Fig. 23. These data are in good agreement on the lower surface and on the upper surface ahead of the shock wave. The position of the shock wave is in excellent agreement between the two experiments with noticeable disagreement in the pressure distributions downstream of the shock wave. The latter could stem from the differences in Reynolds number since the pressure distribution downstream of the shock wave is strongly influenced by the Reynolds number.[23]

To summarize the comparison with Osborne's results, the data obtained at supercritical conditions, Figs. 21 and 23, are in good agreement. The differences in shock position at zero angle of attack, Fig. 21, can probably be attributed to small differences in the Mach number between the two experiments. The data for a supercritical lifting case, Fig. 23, show some differences downstream of the shock wave which probably stem from the differences in the test Reynolds numbers. The data for a subcritical lifting case, Fig. 22, are not in good agreement. Both the upper surface pressure distributions and the lift coefficients differ significantly. Osborne's angle of attack and lift coefficient have been corrected for blockage effects, and this might be a source of the discrepancies.

Similar comparisons have been made with Goethert's pressure distribution data[24] obtained with an NACA 0012 section, but they are not included here. As noted earlier, those data probably were influenced by tip effects. Goethert's data were compared with the present data at small angles of attack ($M_\infty = 0.85$, $\alpha = 0.35°$) and were in reasonable agreement except for the

position of the shock wave. The differences in shock position probably stem from the fact that Goethert's experiments were made with natural transition at a Reynolds number of 6×10^6 and the present experiments were with fixed transition and a Reynolds number of 10^6. It was noted earlier that transonic tests of a two-dimensional 0012 airfoil have been made at the Institut de Mécanique des Fluides in Lille.[6] No comparisons were made with those data because there were no comparable test conditions.

Murman[7] and Krupp[25] have published exact solutions for the lifting 0012 airfoil in free air. They give pressure data for Mach numbers and angles of attack that match those reported here, but they obtain lift coefficients substantially greater than observed here. For example, Murman finds that at $M_\infty = 0.65$ and $\alpha = 2°$, the lift coefficient is 0.345. That value is 37% greater than the value observed here, and is 15% greater than the value one obtains by scaling the classical incompressible value including thickness effects. It would be meaningful to make a comparison at equal lift coefficients, but the present experiments did not include the specific lift coefficients obtained by Murman. Similarly, for $M_\infty = 0.75$ and $\alpha = 2°$, Krupp's solution yields a lift coefficient that is about 22% greater than that observed in the present experiments, and a meaningful comparison cannot be made with the present data.

CONCLUDING REMARKS

A series of subsonic wind tunnel tests has been made with a 6-inch chord, two-dimensional wing with an NACA 0012 section in the Calspan Eight-Foot Transonic Wind Tunnel in order to generate a set of two-dimensional data with minimum wall interference effects on the model. The model has a blockage area of 0.75% of the test section cross-sectional area, and it is estimated from existing theories that the blockage interference was less that 0.1% of the free-stream velocity, and that the lift interference was less than 2% of

the lift coefficient for all Mach numbers that were tested. Boundary layer transition was fixed at 10% of the chord, and all tests were made with a chord Reynolds number of 10^6. The tests were made at Mach numbers ranging from 0.4 to 0.95 and at angles of attack ranging from -2° to +8°. The measurements included three-component forces on a small metric section, pressure measurements on the nonmetric section, and oil flow observations at the wing roots.

The experimental lift curve slopes were scaled to an incompressible value using Prandtl-Glauert and von Kármán-Tsien scaling. The scaled data at the lowest Mach number agreed to within 1% of incompressible theory when the theory is corrected for thickness effects and viscous effects. The lift curves exhibit the expected compressibility effects for Mach numbers below 0.85. The lift curve slopes at small angles of attack were very small for Mach numbers between 0.85 and 0.925 because the shock waves on the upper and lower surface produced a pronounced redistribution of the aerodynamic loads.

The drag data at zero lift show a 14% increase in the subcritical range, and show the critical Mach number is about 0.75; somewhat higher than the theoretical value of 0.725. The subcritical increase in profile drag stemmed from inviscid compressibility effects on the viscous drag. It was found that Prandtl-Glauert scaling effectively removed this effect when applied to a component of the profile drag.

The subcritical pressure distribution data were scaled with the Prandtl-Glauert parameter and the von Kármán-Tsien parameter and agree well with incompressible theory. Supercritical data were compared with other experimental data with good agreement.

REFERENCES

1. Sears, W.R. "Self-Correcting Wind Tunnels" Calspan Report No. RK-5070-A-2 July 1973 (The Sixteenth Lanchester Memorial Lecture, to be published in The Aeronautical Journal)

2. Anon. "Eight-Foot Transonic Wind Tunnel" Calspan Report No. WTO-300 September 1973

3. Priebe, R.W., and Chudyk, D. "Airflow Calibration of the Reflection Plane Cart with Forward and Aft Island Extensions" Calspan Report No. WTO-531 February 1969

4. Lock, R.C. "Test Cases for Numerical Methods in Two-Dimensional Transonic Flows" AGARD Report No. 575 November 1970

5. Osborne, J. "A Selection of Measured Transonic Flow Pressure Distributions for the NACA 0012 Airfoil" RAE Provisional Report (to be published)

6. de Paul, M.V., and Dyment, A. "Recherches sur les Profils d'ailes en Ecoulement Subsonique Eleve" L'Aeronautique et L'Astronautique, Vol. 19 No. 3 1970

7. Murman, E.M. "Computation of Wall Effects in Ventilated Transonic Wind Tunnels" AIAA Paper No. 72-1007 September 1973

8. Halliday, A.S., and Cox, D.K. "Note on the Effect of Size and Position of End Plates on the Lift of a Rectangular Wing in a Wind Tunnel" ARC C.P. 305 1956

9. Van Dyke, M. "Perturbation Methods in Fluid Mechanics" Academic Press, New York 1964 p. 172

10. Vidal, R.J. "The Influence of Two-Dimensional Stream Shear on Airfoil Maximum Lift" JAS Vol. 29 No. 8 August 1962 pp. 889-904

11. Pindzola, M., and Lo, C.F. "Boundary Interference at Subsonic Speeds in Wind Tunnels with Ventilated Walls" AEDC-TR-69-47 May 1969

12. Chew, W.L. "Cross-Flow Calibration at Transonic Speeds of Fourteen Perforated Plates with Round Holes and Airflow Parallel to the Plates" AEDC-TR-54-65 July 1955

13. Braslow, A.L., and Knox, E.C. "Simplified Method for Determination of Critical Height of Distributed Roughness Particles for Boundary Layer Transition at Mach Numbers from 0 to 5." NACA TN 4363 September 1958

14. Goethert, B. "Aerofoil Measurements in the DVL (2.7 M) High Speed Wind Tunnel" Nat. Res. Coun. Report No. TT-31 September 1947

15. Goethert, B. "High Speed Tests on Symmetrical Profiles with Different Thickness Ratios in the DVL High-Speed Wind Tunnel (2.7 M Dia.) and Comparison with Measurements in other Wind Tunnels" Nat. Res. Coun. Report No. TT-38 October 1947

16. Abbott, I.H., von Doenhoff, A.E., and Stivers, L.S. "Summary of Airfoil Data" NACA TR 824 1945

17. Glauert, H. "The Elements of Aerofoil and Airscrew Theory" Cambridge 1943

18. Spence, D.A. "Prediction of the Characteristics of Two-Dimensional Airfoils" JAS Vol. 21 No. 9 September 1954 pp. 577-587

19. Thwaites, B. "Incompressible Aerodynamics" Oxford 1960 p. 196

20. Squire, H.B., and Young, A.C. "The Calculation of the Profile Drag of Airfoils" A.R.C. R & M 1838 1938

21. Spalding, D.B., and Chi, S.W. "The Drag of a Compressible Turbulent Boundary Layer on a Smooth Flat Plate With and Without Heat Transfer" J.F.M. Vol. 18 Pt. 1 January 1964 pp. 117-143

22. Sells, C.C.L. "Plane Subcritical Flow Past a Lifting Aerofoil" R.A.E. T.R. 67146 1967

23. Vidal, R.J., Wittliff, C.E., Catlin, P.A., and Sheen, B.H. "Reynolds Number Effects on the Shock Wave-Turbulent Boundary Layer Interaction at Transonic Speeds" AIAA Paper No. 73-661 July 1973

24. Geothert, B. "Pressure Distribution and Momentum Loss Diagrams for the NACA Profile 0.0012 - 1.130 at High Subsonic Speed" Nat. Res. Coun. Report No. TT-27 May 1947

25. Krupp, J.A. "The Numerical Calculation of Plane Steady Transonic Flows Past Thin Lifting Airfoils" BSRI Report No. D180-12958-1 June 1971